


Article

Interdecadal Variability in Myanmar Rainfall in the Monsoon Season (May–October) Using Eigen Methods

Zin Mie Mie Sein ¹, Irfan Ullah ^{2,*} , Farhan Saleem ^{3,4}, Xiefei Zhi ^{2,5,*}, Sidra Syed ⁶ and Kamran Azam ⁷¹ College of International Students, Wuxi University, Wuxi 214105, China; dr.zin28@gmail.com² School of Atmospheric Science, Nanjing University of Information Science and Technology, Nanjing 210044, China³ College of Earth and Planetary Sciences, University of Chinese Academy of Sciences, Beijing 100049, China; farhan@mail.iap.ac.cn⁴ International Centre for Climate and Environment Sciences, Institute of Atmospheric Physics, Chinese Academy of Sciences, Beijing 100049, China⁵ Weather Online Institute of Meteorological Applications, Wuxi 214000, China⁶ Institute of Peace and Conflicts Studies, University of Peshawar, Peshawar 25000, Pakistan; sidsyed.92@yahoo.com⁷ Department of Management Sciences, University of Haripur, Khyber Pakhtunkhwa 22780, Pakistan; kamran.azam@uoh.edu.pk

* Correspondence: irfan.marwat@nuist.edu.cn (I.U.); zhi@nuist.edu.cn (X.Z.)

Abstract: In this study, we investigated the interdecadal variability in monsoon rainfall in the Myanmar region. The gauge-based gridded rainfall dataset of the Global Precipitation Climatology Centre (GPCC) and Climatic Research Unit version TS4.0 (CRU TS4.0) were used (1950–2019) to investigate the interdecadal variability in summer monsoon rainfall using empirical orthogonal function (EOF), singular value decomposition (SVD), and correlation approaches. The results reveal relatively negative rainfall anomalies during the 1980s, 1990s, and 2000s, whereas strong positive rainfall anomalies were identified for the 1970s and 2010s. The dominant spatial variability mode showed a dipole pattern with a total variance of 47%. The power spectra of the principal component (PC) from EOF revealed a significant peak during decadal timescales (20–30 years). The Myanmar summer monsoon rainfall positively correlated with Atlantic multidecadal oscillation (AMO) and negatively correlated with Pacific decadal oscillation (PDO). The results reveal that extreme monsoon rainfall (flood) events occurred during the negative phase of the PDO and below-average rainfall (drought) occurred during the positive phase of the PDO. The cold phase (warm phase) of AMO was generally associated with negative (positive) decadal monsoon rainfall. The first SVD mode indicated the Myanmar rainfall pattern associated with the cold and warm phase of the PDO and AMO, suggesting that enhanced rainfall for about 53% of the square covariance fraction was related to heavy rain over the study region except for the central and eastern parts. The second SVD mode demonstrated warm sea surface temperature (SST) in the eastern equatorial Pacific (El Niño pattern) and cold SST in the North Atlantic Ocean, implying a rainfall deficit of about 33% of the square covariance fraction, which could be associated with dry El Niño conditions (drought). The third SVD revealed that cold SSTs in the central and eastern equatorial Pacific (La Niña pattern) caused enhance rainfall with a 6.7% square covariance fraction related to flood conditions. Thus, the extra-tropical phenomena may affect the average summer monsoon trends over Myanmar by enhancing the cross-equatorial moisture trajectories into the North Atlantic Ocean.

Keywords: summer monsoon rainfall; interdecadal variability; AMO; PDO; Myanmar

Citation: Mie Sein, Z.M.; Ullah, I.; Saleem, F.; Zhi, X.; Syed, S.; Azam, K. Interdecadal Variability in Myanmar Rainfall in the Monsoon Season (May–October) Using Eigen Methods. *Water* **2021**, *13*, 729. <https://doi.org/10.3390/w13050729>

Academic Editor: Scott Curtis

Received: 26 January 2021

Accepted: 3 March 2021

Published: 7 March 2021

Publisher's Note: MDPI stays neutral with regard to jurisdictional claims in published maps and institutional affiliations.



Copyright: © 2021 by the authors. Licensee MDPI, Basel, Switzerland. This article is an open access article distributed under the terms and conditions of the Creative Commons Attribution (CC BY) license (<https://creativecommons.org/licenses/by/4.0/>).

1. Introduction

Rainfall variability is among the basic indicators of climate and water cycle changes in a region [1]. Anomalous changes in rainfall dynamics may cause hydro-meteorological hazards such as flood, drought, and storms [2,3], thus ultimately resulting in loss of human

lives, and destruction of biodiversity and natural resources [4,5]. Variation in rainfall pattern may also occur on intra-seasonal and inter-annual scales, posing serious threats to agriculture, water resources, and the sustainable development of a region [5,6]. The Intergovernmental Panel on Climate Change (IPCC) stated that global -warming-induced climate change has intensified the variability in rainfall over space and time across the globe [7]. It is also projected that the spatiotemporal variability in rainfall and related extremes will intensify in the near future [7]. These projections can be used as feedback for the policy makers in water resource management, disaster risk reduction, and regional climate analysis [8].

The climate of Myanmar is dominated by the Southeast Asian (SEA) monsoon; about 70% of the total annual rainfall is received during monsoon season (June to September), with large spatiotemporal variance at the country level across latitude and longitude. With high exposure and low resilience, the SEA region is highly vulnerable to climate change influences, especially as the intensity and frequency of extreme events may increase in the near future [9]. Ge et al. [10] showed future projections in rainfall extremes over the SEA using CMIP6 multi-model ensemble. They reported significant changes in the number of heavy rainfall days and the intensity of daily rainfall, demonstrating that locally heavy rainfall is likely to occur over a short time and that more rainfall extremes over the SEA are probable in a warmer future. Such increasing trends in extreme rainfall have been scientifically observed during last few decades over Asia [10,11], and will likely increase further with global warming. Variation in the monthly distribution of monsoon rainfall and its amounts will have a substantial impact on the agricultural production, water resources, and overall economy. It is expected that rainfall intensity shifting and patterns will undergo certain changes, and extreme weather events such as drought and flood may occur more frequently [12]. In recent years, such changes have already been experienced over the SEA, resulting in heavy rainfall and loss of capital, infrastructure, and human lives during 2009 and 2014 in Myanmar [13–15] and the 2015 and 2017 floods in India and Bangladesh [16]. These changes, to some extent, were linked to large-scale anomalous atmospheric circulation patterns and the resultant flux, which caused local and remote damage on a vast scale [17].

The classical division of monsoon areas used at the beginning of the 20th century was entirely based on the annual reversal of winds and increase rainfall during a short period of time [18]. The classical definition binds the monsoon to the eastern hemisphere, including Asian, Australian, tropical African, and Indian Ocean monsoon systems. The simulation experiments and geological records suggest that the Asian monsoon is sensitive to land surface features such as Tibetan uplift and Himalayan terrain [19,20]. Regional variability in magnitude, onset, and withdrawal of monsoonal rainfall is linked to continental, oceanic, and atmospheric circulation patterns [21]. Changes in these features are usually used as an integrated component in the forecast for predicting the above features [22,23]. The IPCC indicated that the impact of climate change on regional monsoon rainfall intensity and variability is more complex and uncertain, and the near-future monsoon system may be more severe than in the present decade [11].

Numerous studies have been conducted in Myanmar to identify the spatiotemporal trends in monthly, annual, and seasonal rainfall [21,24]. These variations strongly affect the ecological, social, and economic aspects of the country, such as availability of water resources, agricultural production, and economic practices [25,26]. A recent study indicated that the seasonal monsoon rainfall exhibits an increasing trend in the northwest of Myanmar, but a decreasing trend in the southern coastal belt [27,28]. The monsoon rainfall showed an upward trend in southeastern Myanmar, but a downward trend in the central parts [29]. The northern and northeastern plateau of Myanmar experienced an increasing trend in monsoon rainfall [30]. It has been projected that the interannual variation in monsoon rainfall will continue in the future with significant intensity, which will adversely impact the climate and hydrometeorological aspects of Myanmar [4,31]. Chhin et al., (2019) proposed an area-averaged sea surface temperature (SST) and a combination of different

variables at each corresponding location over an equatorial region, and found a good predictor for operational long-term statistical prediction of monthly rainfall in the southern Indochina Peninsula, particularly for the pre-monsoon season. The aforementioned studies provided detailed information about the spatiotemporal changes in monsoon rainfall over Myanmar; however, none of the studies considered the sub-seasonal rainfall variation. Furthermore, the perceived potential drivers of monsoon variability have also not been explored in detail in the region [17,32].

According to Zaw et al., (2020), extreme events are associated with the broader-scale atmospheric circulations of the Pacific and Indian Oceans, especially during the positive phase of the El Niño southern oscillation (ENSO). Long-term climate variation affects seasonal to interannual climate variability and is important in the climate research over the SEA region, mainly over Myanmar. In this study, the empirical orthogonal function (EOF) method was used to analyze the decadal timescales of the dominant mode of the monsoon rainfall pattern. The extreme behavior of summer monsoon rainfall variability, which is related to global climate phenomena such as the Pacific decadal oscillation (PDO) and the Atlantic multidecadal oscillation (AMO), was analyzed using the singular value decomposition (SVD) method. After this, we examined the correlation between summer monsoon rainfall and SST on the decadal time scale. We aimed to fill the gap in the literature by assessing the interdecadal variability in summer monsoon rainfall to identify the relevant large-scale phenomena of the atmospheric and oceanic circulation. The summer monsoon mostly occurs during the months of May to October in the study region. Therefore, we considered May to October in our investigation of the monsoon season influence over Myanmar from 1950 to 2010 [4,33,34]. The rest of this paper is structured as follows: Section 2 describes our data and methodology; the results are provided in Section 3, with the discussion and conclusions presented in Section 4.

2. Study Area

Myanmar is a tropical country situated in the SEA region at 9°–28° N and 92°–101° E (Figure 1). SEA is located in Asia, comprising the south of China, the east of India, and the northwest of Australia. The region is located between the Indian Ocean and the Bay of Bengal (BoB) in the west, the Philippine Sea, the South China Sea, and the Pacific Ocean in the east [35]. Myanmar's climate is mostly influenced by the Indian summer monsoon [36]. The country has a tropical to subtropical monsoon climate with three seasons: hot, dry inter-monsoonal (mid-February to mid-May); rainy southwest monsoon (mid-May to late October); and cool and dry northeast monsoon (late October to mid-February) (NAPA, 2012). Myanmar is an agricultural country and monsoon rice occupies 80% of the planted rice area; for summer rice, it occupies 20% [37]. The region is located in the Indian monsoon regions where weather and climate disasters frequently produce damage in the summer monsoon season (May–October). For example, in 2019 and 2020, extreme floods and landslides in Myanmar occurred due to the strong monsoon rainfall, resulting in considerable loss of life and property. Long-lasting extremely dry periods and the very low amount of total monsoon rainfall (May–October) affect water scarcity and threaten the economy, livelihood, and food security in the country [4,31]. Water scarcity occurs in the central dry and deltaic regions during the summer (March–April) [38].

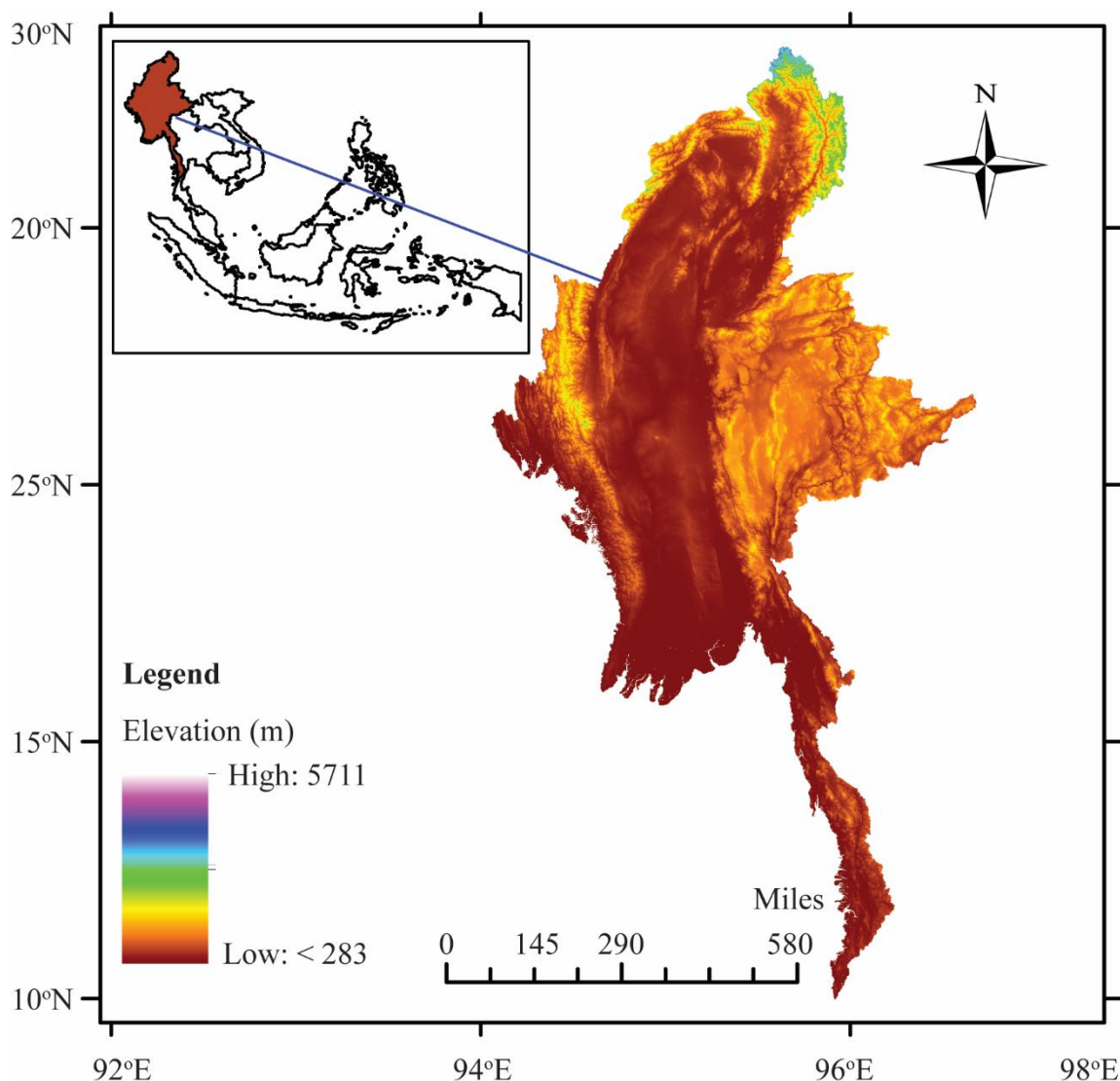


Figure 1. Elevation map of the study area.

3. Data and Methodology

3.1. Data

We used monthly gauge-based gridded rainfall datasets of the Global Rainfall Climatology Centre (GPCC) and Climatic Research Unit version TS4.0 (CRU TS4.0) during the period of 1950–2019 [39–42]. The gridded climate datasets were collected with a spatial resolution of $0.5^\circ \times 0.5^\circ$ over the study region. Several institutes have developed gridded climate datasets during the past few decades, which are frequently used in hydro-climatic assessments [40,43,44]. Among others, the data products of CRUTS4.0 and GPCC are commonly used due to a longer temporal span [39,41]. The in situ observation data of 35 meteorological stations were acquired from the Department of Meteorology and Hydrology (DMH), Myanmar. The long-term in situ observation data were further used after validation with observed summer monsoon rainfall (1950–2019), which is highly correlated with GPCC gridded data, to investigate the interdecadal variability.

The monthly data of the Pacific decadal oscillation (PDO) Index from May–October for the period 1950 to 2010 were used in this study [22,45]. The AMO index is defined as a local estimate over the entire North Atlantic low-resolution annual SST anomalies after removing any direct trend [46]. The North Pacific (NP) index, North Atlantic Oscillation (NAO) index, and the Arctic Oscillation (AO) index data were also used in this

study [47]. Large-scale atmospheric circulation, such as air temperature and relative humidity, was collected from ERA5 the 5th generation reanalysis of the European Centre for Medium-Range Weather Forecasts (ECMWF) to determine the related breakouts and their moisture transport [48,49]. The extended version of the Reproduced Ocean Surface Temperature (ERSST, version3b), published in the National Maritime and Barometrical Administration/National Climatic Information Center, was used for seawater heating [50]. Analytical data from the National Centers for Environmental Prediction/National Center for Atmospheric Research (NCEP/NCAR) [51], such as speed, zonal and meridional wind, vertical speed ($0.5^\circ \times 0.5^\circ$), were used to explore long-term wind zones.

3.2. Methods

The EOF is a statistical method broadly used to minimize the multidimensionality of complex climate information and recognize the most imperative physical modes with the least chance of data being misplaced [52,53]. Principal component analysis (PCA) is used for the assessment of atmospheric information based on the EOF method [54]. The technique describes the variance and covariance of the data, describing a few modes of variability. The modes that explain the largest percentage of the original variability are considered significant. The modes can be represented by orthogonal spatial patterns (eigenvectors) and corresponding time series (principal components). The EOF technique has been successfully used in Myanmar to investigate the interannual variability in summer monsoon rainfall [25]. With regard to the temporal behavior of the EOF mode, a 10-year running average was applied to obtain the long-term variability. The summer monsoon rainfall data were normalized to prevent areas and seasons of maximum variance from dominating the eigenvectors [55]. The standardized rainfall values were computed for all the years from the long-term mean, yearly mean, and the standard deviation using Equation (1):

$$Z = \frac{X - \bar{X}}{S_d} \quad (1)$$

where Z represents the standardized departure, \bar{X} is the long-term mean value, and S_d is the standard deviation from the mean. The Z value provides immediate information about the significance of a specific deviation from the mean [25,56].

The orthogonal function of EOF is defined as:

$$z(x, y, t) = \sum_{k=1}^N PC(t) \times EOF(x, y) \quad (2)$$

where $z(x, y, t)$ denotes the function of space (x, y) and time (t), while $EOF(x, y)$ represents the spatial structure in relation to the temporal variation in Z .

A power spectrum was analyzed to evaluate the multiscale temporal variations resulting from the wavelet transform employed in the long-term rainfall dataset [57–59]. The decadal spectra were used to estimate the changes that occur in the rainfall pattern on a decadal basis. Prior to performing the power spectrum analysis from the results of the EOF, PCA was used to verify the significance of the scales of interdecadal variation in this study. The red noise spectrum of the decadal spectrum was computed [54]. The confidence limits related to the read noise spectrum were calculated with 90% confidence levels.

Composites include classifying and averaging one or more category of the variable fields according to their relation with the prevailing situations [60]. Composites results are used to produce hypotheses for patterns related to individual scenarios [53,61]. The goal of the composite analysis was to produce the wet and dry years separately. It is primarily used in China and Myanmar to detect the circulation anomalies connected with wet/dry events [25,45,62].

Horizontal moisture transfer rate/flux convergence (MFC), known as moisture convergence, was identified for wet and dry years using the vector character. The MFC results

from the conservation of water vapor in pressure coordinates, which has been discussed in detail previous [63]. MFC can be calculated as:

$$MFC = -\nabla \cdot (qV_h) = -V_h \cdot \nabla q - q \nabla \cdot V_h \quad (3)$$

where $\nabla = \hat{i} \left(\frac{\partial}{\partial x} \right) + \hat{j} \left(\frac{\partial}{\partial y} \right)$, q is the specific humidity, and $V_h = (u, v)$.

The nonparametric Mann–Kendall test (MK) test was used to detect the trend in monsoon rainfall [64,65]. The MK test is widely used to evaluate trends in rainfall, agrometeorological, and hydrological time series [66–72]. This trend test's limitations are normally associated with its own null hypothesis, which assumes that the data are independently and identically distributed. However, the null hypothesis is commonly taken as evidence of the null hypothesis, which is commonly used as evidence of a trend in a given agrometeorological and/or hydrological time series. The MK test investigates the sequential change point to emphasize an abrupt change significant at the 95% confidence level. This approach has been used successfully worldwide [70,73,74] to detect climate variables' change points. For certain datasets consisting of x values with a sample size Sen slope (SS), the MK calculation begins by estimating the S statistic as:

$$S = \sum_{i=1}^{SS-1} \sum_{j=i+1}^{SS} \text{sgn}(x_j - x_i) \dots \text{for } j > i \quad (4)$$

As presented in Mann (1945) and Kendall (1975), when $SS \geq 8$, the distribution of S approaches the Gaussian form with mean $E(S) = 0$ and variance $V(S)$ is calculated using:

$$V(S) = \frac{SS(SS-1)(2SS+5) - \sum_{m=1}^{SS} ti(m-1)(2m+5)m}{18} \quad (5)$$

where ti is the number of ties of length m .

The S statistic is standardized Z , as shown in Equation (6), and its significance can be estimated from the normal cumulative distribution function.

$$Z = \begin{cases} \frac{S-1}{\sqrt{V_s}} \rightarrow S > 0 \\ 0 \rightarrow S = 0 \\ \frac{S+1}{\sqrt{V_s}} \rightarrow S < 0 \end{cases} \quad (6)$$

Singular value decomposition (SVD) analysis is used in two techniques: meteorological and oceanographic data analysis. SVD is applied between two identical datasets of two jointly analyzed fields to identify pairs of the coupled spatiotemporal variations. Bretherton et al., (1992) [75] and Wallace et al., (1992) [76] provided a brief introduction to the SVD method as a fundamental matrix operation that can be considered an extension of rectangular matrices of the diagonalization of a square symmetric matrix. In the calculation, each pair defines the covariance percentage between the two joint fields, allowing the extraction of the dominant modes of pair covariability between the two analyzed fields. Moreover, the SVD of the cross-covariance matrix identifies from two data fields pairs of spatial patterns that explain as much as possible of the mean-squared temporal variance between the two fields. This method is widely used [25] because it works on common and ambiguous data sets. In this work, SVD was used to find the maximum covariance or correlation between the summer monsoon rainfall over Myanmar and the SST over the Indian Ocean and Pacific Ocean.

After this, we used ensemble empirical mode decomposition (EEMD), which is an adaptive time-frequency data analysis technique developed by Wu et al., (2007) [77] and Wu and Huang (2009) [78]. It is used to resolve problems of mixed-mode and false components in the empirical mode decomposition (EMD) decomposition process. This method is a major modification of the original EMD method, emphasizing the adaptiveness and temporal locality of the data decomposition [79]. The EMD method can decompose

any complicated data series into a few amplitudes of frequency-modulated oscillatory components, called intrinsic mode functions (IMFs), of distinct timescales [80]. EMD is based on the local characteristic time scale of a signal, and decomposes the complicated signal into a number of IMFs. The main steps of the EEMD method employed in this study were similar to those outlined by Qian (2009) [81,82]. In this study, EEMD was used to decompose the summer monsoon rainfall and PDO index.

4. Results

4.1. General Characteristics of Monsoon Rainfall

4.1.1. Annual Cycle

The climatological annual cycle of the monthly mean monsoon rainfall over Myanmar (1950–2019) was estimated based on: in situ observation, CRUTS4.0, and GPCC datasets; the results are shown in Figure 2. The error bars show the monthly standard deviation of climatological annual cycle with in each active and break spells. The horizontal solid lines show the monthly standard deviations of all datasets with blue, grey, and orange bars. Interestingly, the significant number of active spells (blue and orange bars) show positive rainfall pattern from June to August whereas the break spells show relatively weak rainfall pattern during September to October. Table 1 reveals the amount of average monthly summer monsoon rainfall (May–October) from in situ observations, CRUTS4.0, and GPCC for the period of 1950–2019. The country experienced a relatively high unimodal rainfall pattern in June, July, and August, observed in all datasets. The average monthly rainfall from in situ observations was 480 mm in June, 520 mm in July, and 524 mm in August. From GPCC, these amounts were 478, 519, and 519 mm, respectively. The rainfall from CRUTS4.0 exhibited a weaker pattern in these three months (444, 466, and 476 mm, respectively). The higher rainfall agrees with the northern hemisphere summer and monsoon season. The rainfall season in Myanmar extends from May to October, and the rainfall season coincides with summer monsoon onset in the country, which generally occurs in the third week of May. Similar monsoon onset periods were observed by Sein et al., (2015) in a simulation study using Regional Climate Model (RegCM3). Notably, the GPCC dataset produced more accurate results compared to the in situ observations. CRUTS4.0 reported less rainfall compared to the in situ observations and GPCC. We found a strong correlation (0.94) between the in situ observations and GPCC datasets, but a relatively weak correlation (0.52) between the in situ observations and the CRUTS4.0 dataset (Table 2). The root mean square error (RMSE) for GPCC (14.24) for summer rainfall was lower than that of the CRUTS4.0 dataset (45.29) (Table 2). Therefore, GPCC was thus used in most analyses since the data are continuous and can be extrapolated to cover all parts of the country to identify longer time periods. Roy et al., (2011) studied the interannual variability in summer monsoon rainfall in relation to Indian Ocean Dipole (IOD) and ENSO using the GPCC dataset. Therefore, the use of GPCC data provided better results, due to extended longer periods, which were more complete as compared to the observed data.

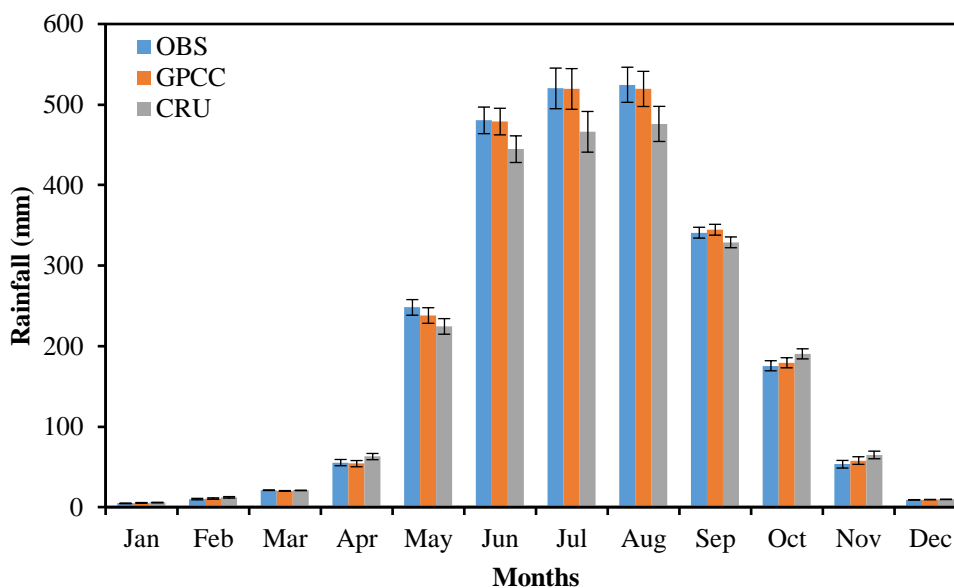


Figure 2. The annual cycle of mean rainfall from in situ observations (OBS), GPCC, and CRUTS4.0 over Myanmar (mm) (1950–2019). The error bars show the monthly standard deviation of the interannual variability within the periods. The horizontal solid lines shows the standard deviation of all datasets blue, grey, and orange bars.

Table 1. Monthly average of the summer monsoon rainfall (mm) from in situ observations, and Global Rainfall Climatology Centre (GPCC) and Climatic Research Unit version TS4.0 (CRUTS4.0) datasets. The bold values represents the significance level (0.05).

Month	In Situ	GPCC (mm)	CRUTS4.0 (mm)
Jan	4.66	5.28	5.60
Feb	9.94	10.54	12.12
Mar	20.93	20.19	20.72
Apr	55.25	53.95	62.75
May	248.03	237.92	224.41
Jun	480.32	478.80	444.51
Jul	520.03	519.32	466.11
Aug	524.53	519.38	475.89
Sep	340.86	344.49	328.81
Oct	175.52	179.23	190.30
Nov	53.25	57.80	64.77
Dec	9.10	9.36	9.54

Table 2. Summary of correlation and root mean square error (RMSE) among GPCC and CRUTS4.0 datasets and in situ observation stations’ data over Myanmar.

Dataset	Correlation Coefficient (R)	RMSE
GPCC	0.94	14.24
CRUTS4.0	0.52	45.29

4.1.2. Climatology of Summer Monsoon Rainfall

Figure 3 shows the climatology of observed May–October mean monsoon rainfall over Myanmar (Figure 3a) and GPCC rainfall (Figure 3b) for the period of 1950 to 2019. Both datasets showed relatively similar spatial rainfall patterns over the country (Figure 3). Maximal rainfall was received along the western coast (Rakhine State), and southern (Mon, Kayin States and Tanintharyi Region) and northern tips (Kachin State) of Myanmar. This aligns with the recent extreme events (floods, strong winds, and landslides) that have occur in these areas due to the strong monsoon rainfall. Along the coastal area (west and south),

regions close to the BoB, Andaman Sea, and northern tip (Kachin State) occupy the highest mountain, called Hkakabo Razi. The central (dry zone) and eastern areas receive less rainfall than other places in the region. The central dry zone receives the lowest amount of rainfall compared to rest of the study area (Figure 3). The observed low rainfall in the central dry zone is attributed to the topography: the area is situated between two mountain ranges: the Shan Plateau to the east and Rakhine Yoma Mountain to the west. Kumar et al., (2006) indicated that increased rains on the Myanmar coast contribute more than total rainfall in the West Ghats, associated to the central and northern regions.

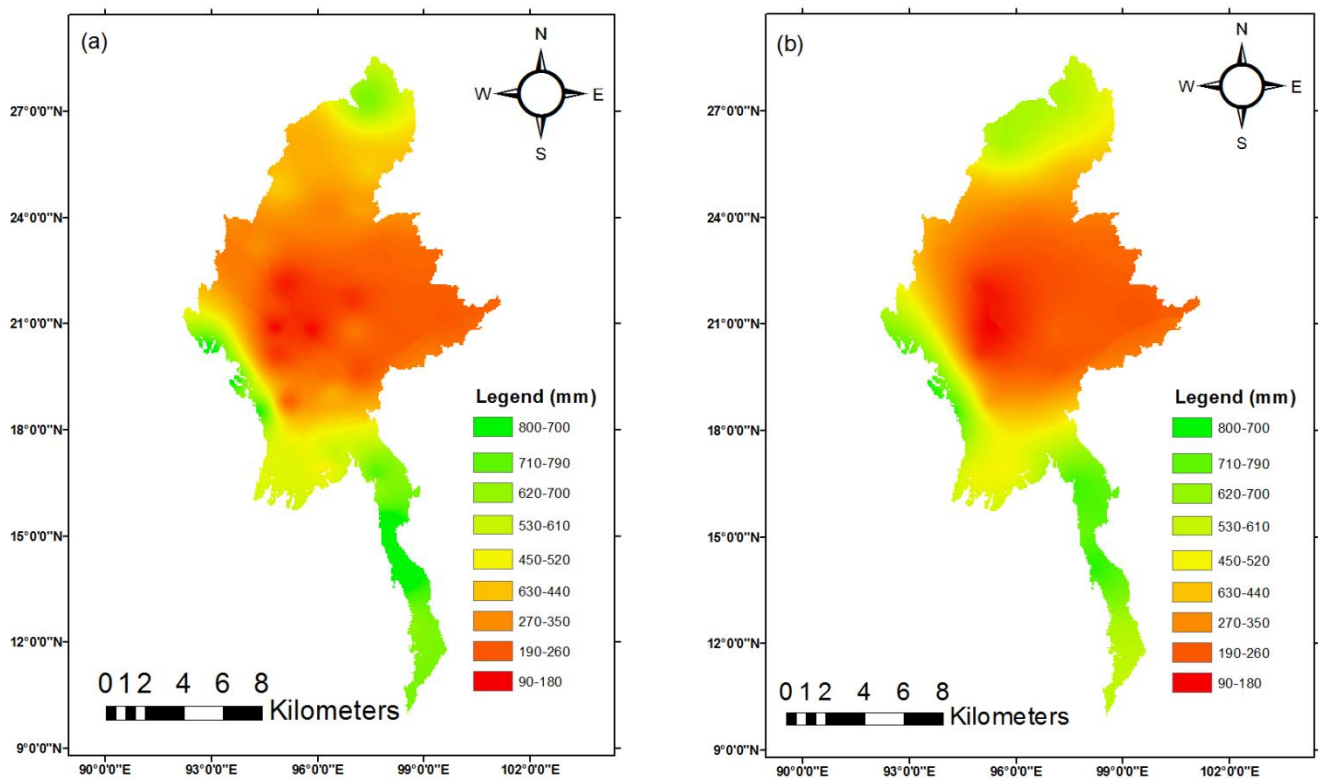


Figure 3. Climatology of mean summer monsoon (May–October) rainfall (mm) over Myanmar (1950–2019) (a) in situ observation rainfall; (b) GPCP rainfall.

4.2. Spatial and Temporal Interdecadal Variability in Summer Monsoon Rainfall.

The change in decadal mean May–October rainfall from the long-term mean rainfall over Myanmar was estimated using GPCP data (Figure 4). In the six decades, the results show strong negative anomalies during the periods of 1971–1980, 1981–1990, and 1991–2000 (Figure 4c–e). From the results, the highest frequency of rainfall occurred during the period 1961–1970, followed by 2001–2010, suggesting frequent extreme rainfall in the recent decade, whereas 1981–1990 and 1991–2001 showed the maximum displacement toward the right side of the figure, indicating an increase in the maximum intensity of monsoon rainfall in the region. Figure 4a,b indicates less rainfall in the western and central parts of Myanmar; however, the opposite was true: the patterns in Figure 4d,e exhibit strong negative change anomalies. Sein et al., (2015) studied ENSO associated with summer monsoon rainfall. They found that most of the El Niño years showed strong negative decadal rainfall anomalies in Myanmar. In addition, strong positive anomalies were recorded in 1961–1970 and 2001–2010 (Figure 4b,f). The results further support the findings of Zaw et al., (2020), who reported that the occurrence of extreme events (i.e., drought and flood) is significantly associated with large-scale atmospheric circulations of the Pacific and Indian Oceans, particularly during the positive phase of the ENSO. The overall strong and positive decadal rainfall anomalies occurred in La Niña years over the

target region. Table 3 reveals that the observed extreme rainfall between 1950 and 2019 occurred in the first three decades for the west coast (Rakhine State), for two decades along the south coast (Tanintharyi Region), and for one decade in the Upper Sagaing Region. This result agrees with the spatial decadal monsoon rainfall in Figure 4.

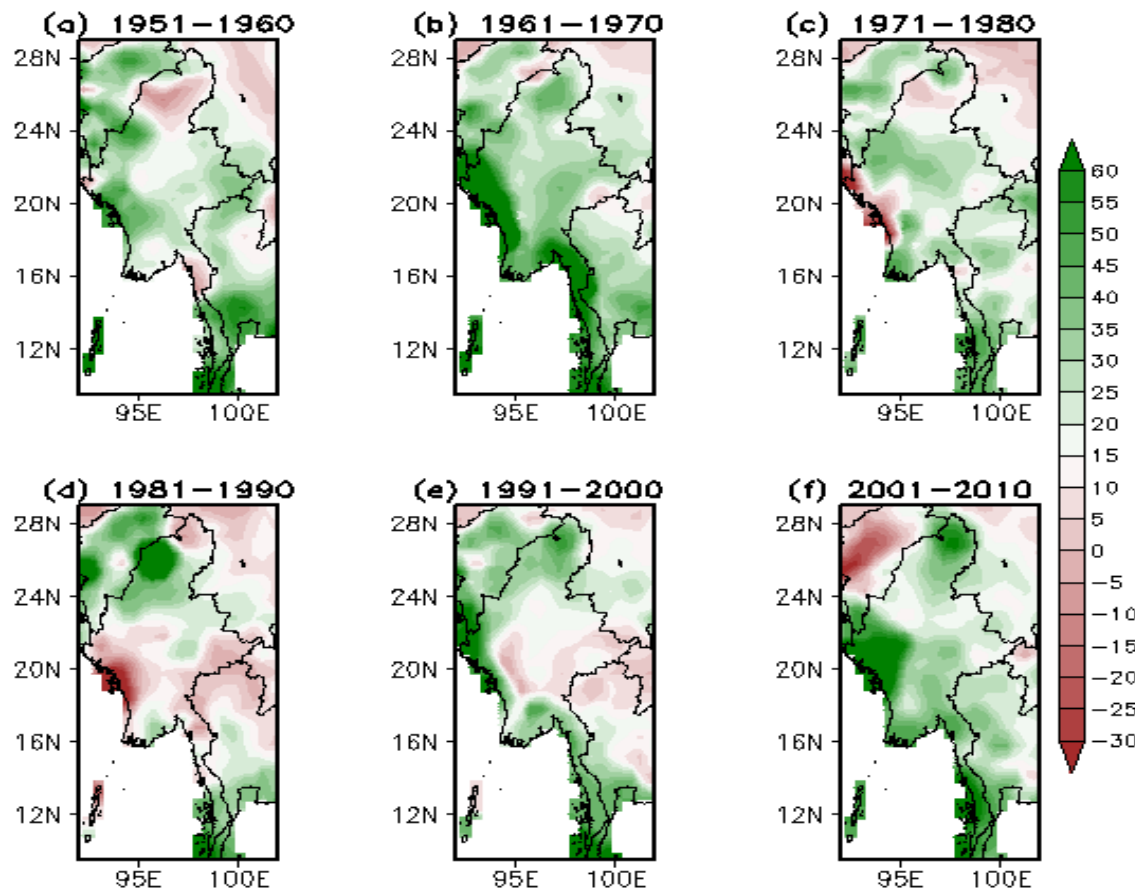


Figure 4. Decadal change in mean summer monsoon rainfall (mm) over Myanmar: (a) 1951–1960; (b) 1961–1970; (c) 1971–1980; (d) 1981–1990; (e) 1991–2000; (f) 2001–2010.

Table 3. Observed extreme decadal rainfall over Myanmar during the period of 1950–2019.

Sr. No	Year	Station	Region/State	Rainfall (mm)
1	4.9.1965	Kyaukpyu	Rakhine	568
2	24.8.1997	Dawei	Tanintharyi	549
3	29.6.1989	Hkamti	Upper Sagaing	527
4	4.7.2006	Dawei	Tanintharyi	447
5	5.6.1980	Sittwe	Rakhine	422
6	18.7.1956	Thandwe	Rakhine	353

From Figure 4 and Table 3, the decadal rainfall fluctuated during the period of 1950–2019, with a positive skewness and increased frequency in recent decades. This suggests an increase in the extreme rainfall events with increased frequency in all study regions, especially in the western and southern regions. This may be associated with increased global-warming-induced changes in monsoon and circulation patterns in the regions; similar rainfall patterns were previously reported [83].

The results for various regions in Myanmar revealed that the west, south, and north regions received the most rainfall, while the east and central regions received relatively less (Figure 5). Figure 5 shows that an overall increasing trend in rainfall occurred over all regions, which corresponds to previously reported findings [18,84,85]; however, the

annual rainfall variability on the regional scale differed. In the northern part, the rainfall variability appeared to be increasing, with an amount of 500 mm. The peak rainfall years (dry years) were recorded during 1992, 1997, and 2010 (1982, 1991, 2005, and 2009). In the eastern part, monsoon rainfall slightly increased, as depicted by a rainfall amount of 250 mm with dry and wet years appearing to be the possible reason for balancing the overall trend in the region. In this region, the highest (lowest) monsoon rainfall was observed in 1988 and 2013 (1987 and 2009). In the central part, the monsoon rainfall exhibited an increasing trend at the rate of 300 mm per year. The analysis showed that 1960, 1997, 2010, and 2014 (1987, 1991, 1999 and 2009) were the peak wet (dry) years in the northern and central parts. Our results concur with the findings of Zaw et al., (2021), who found that 2–4 year high-frequency periodicities from spectral peaks, and predominant regions of high spatial correlations indicated the summer rainfall in Myanmar is associated with large-scale atmospheric circulations, mainly linked with the ENSO events due to SST deviations in the tropical Pacific Ocean. The variations in the western region's dry condition were observed in the late 1960s and 1980s (Figure 5d) and in the late 2000s in southern region (Figure 5e). In the western part, the monsoon rainfall experienced an increasing trend initially with an amount of 250 mm, but a decreasing pattern in the last few decades. In the southern part, the opposite pattern to the western region was observed, recording the highest rainfall (530 mm) over last decades, being the highest amongst all regions. The maximum (minimum) rainfall was recorded in 1960, 1980, 1998, 2006, and 2011 (1987, 1991, 1999, 2002, 2004, 2005, and 2014) in the region.

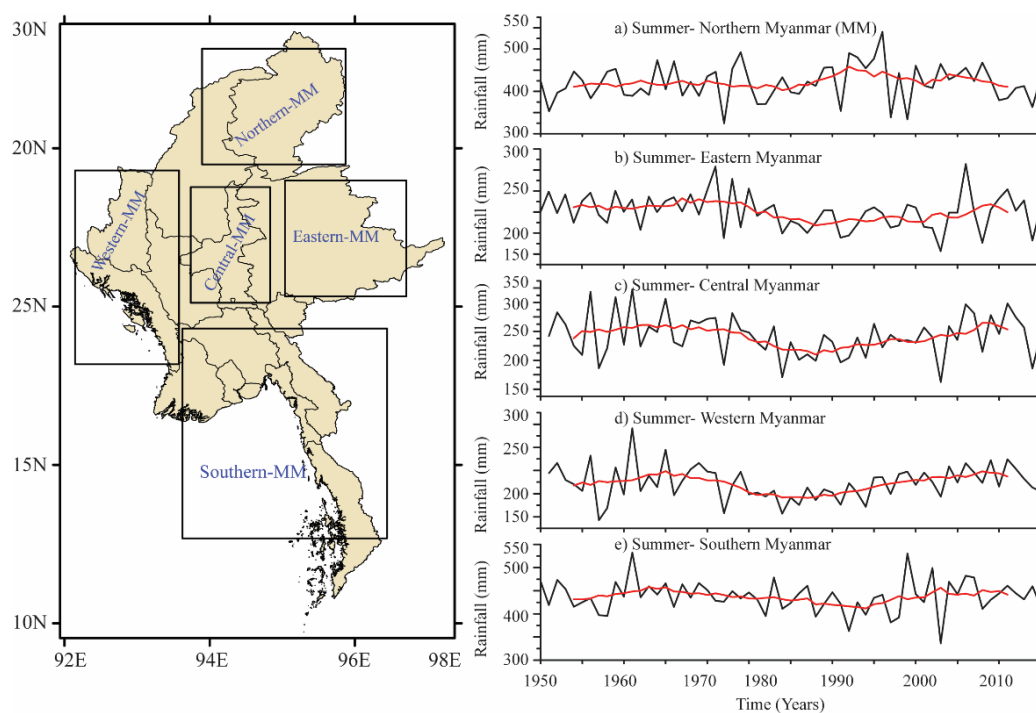


Figure 5. Black lines, homogeneous regions' average summer monsoon rainfall time series (mm); red line, the corresponding 10 year running mean variations (mm): (a) north, (b) east, (c) central, (d) west, and (e) south regions in Myanmar.

The time series of interdecadal variability in rainfall over the whole region is shown in Figure 6. The mean rainfall was observed to increase in the late 1950s, reaching its peak around 1965, and subsequently decreased during the mid-1980s before increasing again in the early 1990s. The second climax was observed in the early 2000s; however, the rainfall decreased in the recent decade. We classified wet and dry years based on the standardized rainfall anomaly as ≥ 1 and ≤ -1 for wet and dry years, respectively. The same approach was used effectively by other authors (Chen and Huang, (2017) in China, Lone et al., (2019) in India, and Sein et al., (2015) in Myanmar). The wet periods were 1962–1967, 1998, 2003,

and 2004; typical dry years were observed during the periods of 1978–1986 and 1988–1990. The results from the sequential Mann–Kendall test statistic were calculated for interdecadal rainfall variability over the region to detect the statistically significant turning points in the decadal trend in rainfall (Figure 7). An abrupt interdecadal change was noted during the 1970s; however, there was a significant reduction (at the 95% confidence level) in rainfall between the 1980s and 2000s (Figure 7), which agrees with spatial map shown in Figure 4.

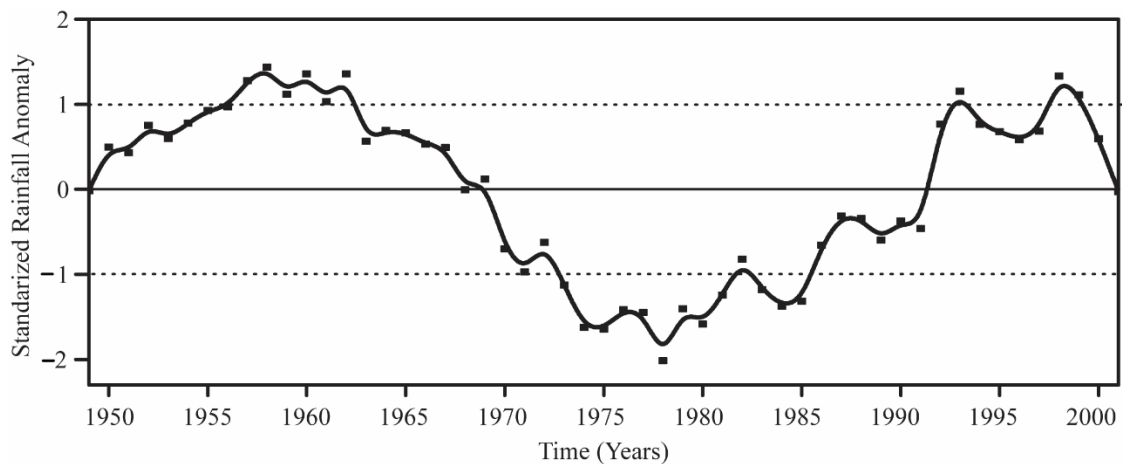


Figure 6. Interdecadal variability estimated with a 10 year running mean of the standardized summer monsoon rainfall (mm) anomaly over Myanmar.

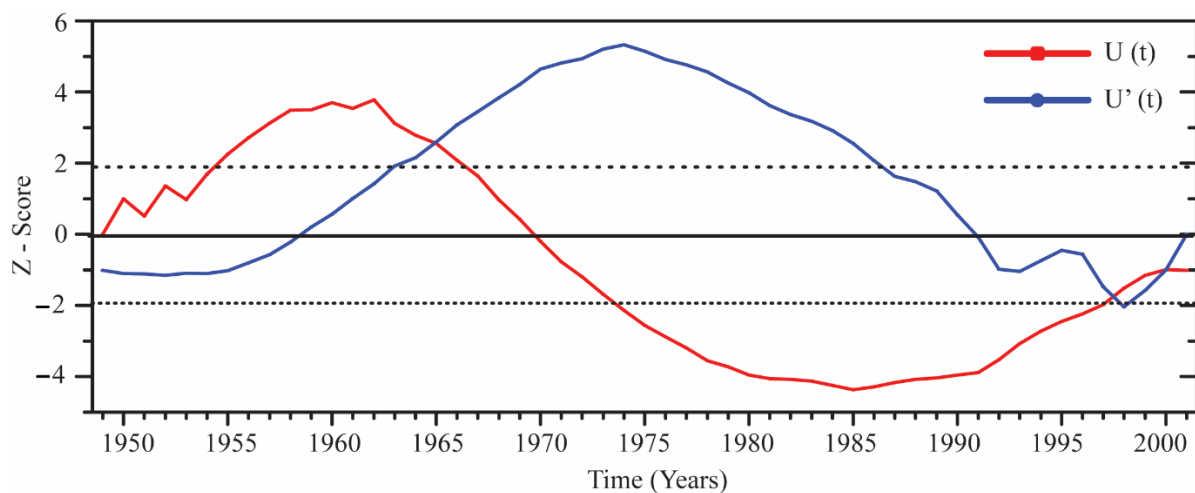


Figure 7. Abrupt change in summer monsoon rainfall derived from the sequential Mann–Kendall test statistic; $U(t)$, forward sequential statistic; $U'(t)$, backward sequential statistic; the upper and lower dashed lines represent significant at the 95% confidence level.

Figures 6 and 7 show that regional variability in monsoon rainfall over Myanmar was obvious during the 1950–2019 period. The magnitude of the rainfall variability could possibly be associated with the geographical location of the region and monsoon circulation patterns. The temporal trend in the Asian and Indian monsoon system showed a strong variation on different time scales, including monthly, inter-annual, intra-seasonal, and annual time scale [18,84,85]. Such large-scale variation due to different factors could induce changes in monsoon rainfall over the diverse study regions [21,86,87].

4.3. Interdecadal Variations in Rainfall and Associated Circulation Influences

4.3.1. Interdecadal Rainfall Variability

The EOFs were examined with the first three eigenvectors of the summer monsoon rainfall in Myanmar for the decadal 10 year running mean (Figure 8). In Myanmar, EOF approaches have been used to detect the interannual variability in summer monsoon rainfall [31,83]. These methods are suitable for finding the total variance in monsoon rainfall in the region. The results reveal that the first EOF (EOF1), explaining 47% of the total variance, showed a dipole spatial pattern with positive loading on the western coast (Rakhine region) and negative loading in northwestern region (Sagaing Region) over the target region (Figure 8a, top and bottom), and explained the corresponding PC-1, which clearly exhibited interdecadal variability. EOF2, explaining 18% of the total variance, exhibited a dipole pattern, with the opposite pattern to EOF1 (Figure 8b, top and bottom), revealing that the PC time series is related to EOF2 (PC2). The third EOF (EOF3), explaining 11% of the total variance, showed strong positive loading in the southern region, and the time series of the consistent PC is connected to EOF3 (PC3), as shown in Figure 8c. To validate the significance of the scales of interdecadal variation, we used the power spectrum from the results EOF: the PC for 53 years was analyzed (Figure 9). PC1–PC3 exhibited a significant spectral peak detected at nearly 20–30 year time scales.

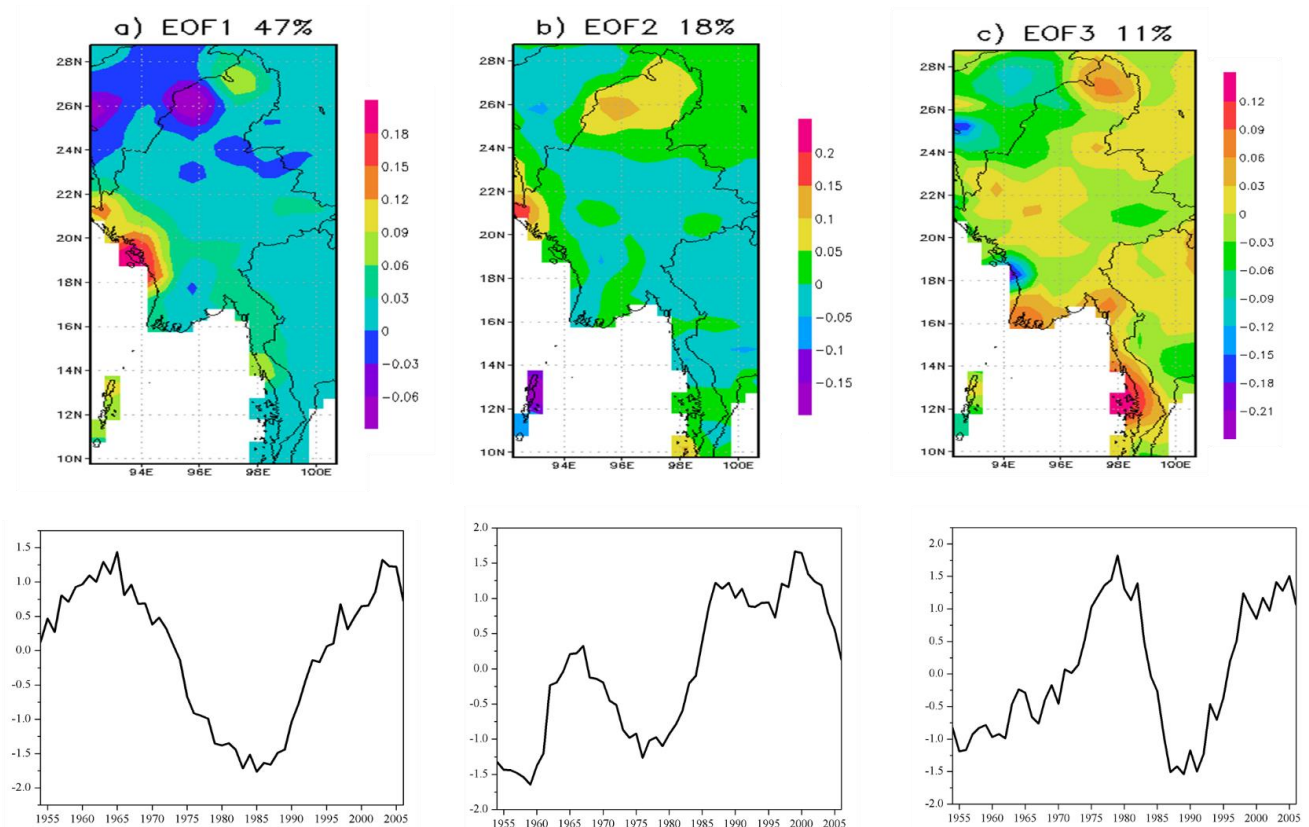


Figure 8. The first three empirical orthogonal functions (EOF_ (top) spatial modes and EOF (bottom) time series: (a) EOF-1, (b) EOF-2, and (c) EOF-3.

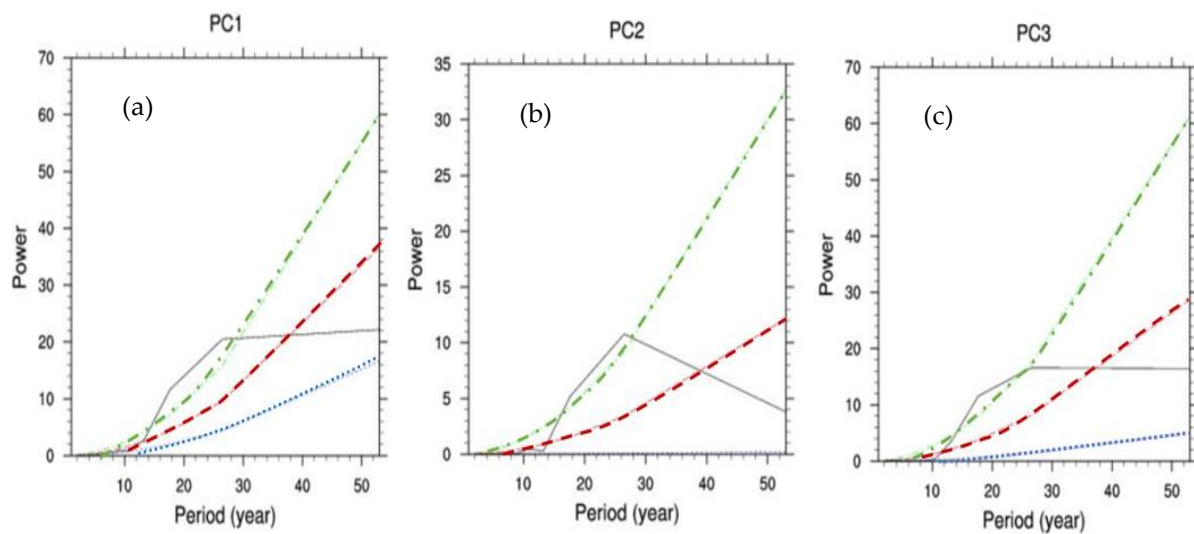


Figure 9. Power spectra: (a) principal component (PC)1, (b) PC2, and (c) PC3. The red line indicates the Markov red noise spectrum, the green dashed line represents the 90% significance, and the blue dashed line denotes the 10% significance boundary for the Markov analysis.

From Figures 8 and 9, we inferred that the interdecadal rainfall pattern over Myanmar has significantly changed over the study period, especially during EOF2 and EOF3. PC1 and PC2 experienced an increasing spectrum over the target region during the period 1950–2019. The humid regions of the country appeared to experience decreasing rainfall, as can be seen in Figure 8c, while the arid regions in the northwestern area experienced an increase in monsoon rainfall. The humid central region appeared to be the core monsoon region of Myanmar; thus, this could imply a shift toward the northwestern parts of the country. Further studies with more data and modeling approaches are needed to validate the current hypotheses.

4.3.2. Large-Scale Atmospheric Circulation Pattern

Rainfall variability is influenced by atmospheric circulation, geographical location, and low latitude in a country like Myanmar. In this section, the general circulation anomalies over low latitudes are examined as a major issue. Circulation patterns on an interdecadal scale are analyzed over the region. To examine the interdecadal variability in the country's rainfall related to the typical circulation patterns on the interdecadal time scale, we employed a low level of horizontal and vertical wind anomalies of 850 hPa for the wet and dry periods (Figure 10). The results show a significant negative westerly or southwesterly winds anomaly from the BoB and Andaman Sea over almost the whole region except the eastern and southern parts during wet years, as shown in Figure 10a. During dry years (Figure 10a), significant negative northeasterly and easterly wind anomalies prevailed in the region. The southwesterly and BoB appeared, which are assumed to be the prime sources of oceanic water transport to continental land masses for rainfall during monsoon seasons (Figure S2). A similar pattern was observed for wind anomalies, further explaining dry conditions and elevated air temperature due to less rainfall. The continental land mass of South East Asia (SEA) experiences a strong anticyclonic pattern, which (in the northern hemisphere) is associated with decreased wind and rainfall. The anticyclonic pattern appeared to be pushing the cyclonic activity toward the tropical region and northern parts of the BoB by pushing the south easterlies to the peninsular tip of India (Figure S2).

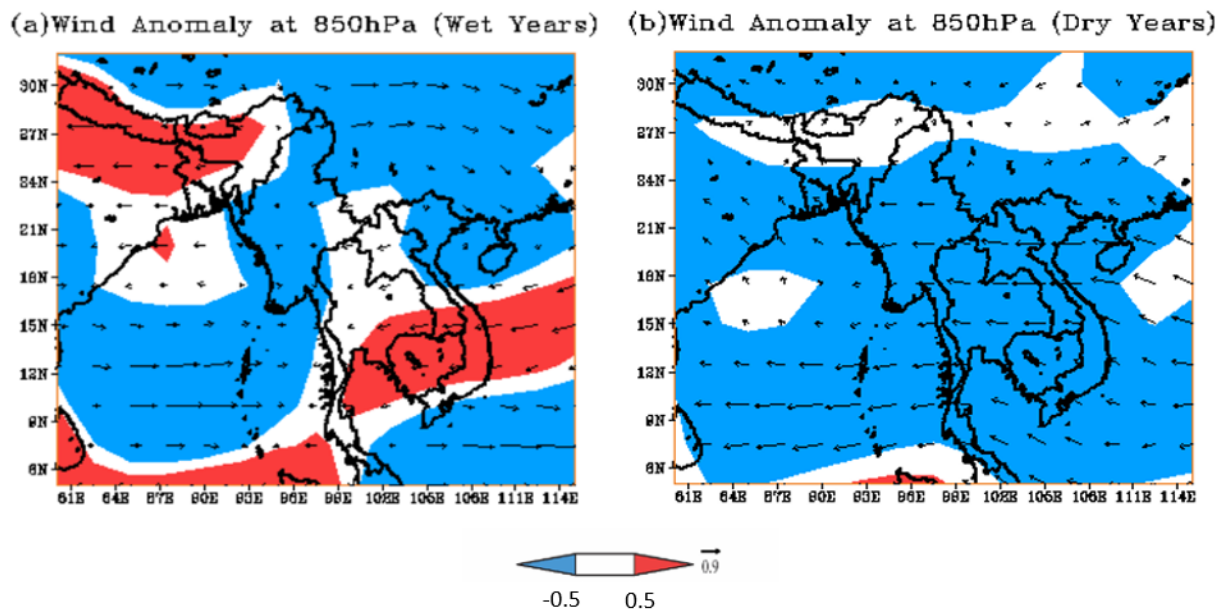


Figure 10. The mean summer monsoon season (May–October) wind anomalies (m/s) at 850 hPa for (a) wet years (1962–1967, 1998, and 2003–2004) and (b) dry years (1978–1986 and 1988–1990). The red (blue) color indicates the significant positive (negative) anomalies over the target region.

During wet years (Figure 10b), the subtropical and Somali jet streams appeared to be pushing the oceanic moisture-rich winds toward the continental land mass. The southern region received northeasterly and easterly winds from the South China Sea, which is the core region experiencing monsoon rainfall. However, the anomalous cloud liquid water contents were obvious over the Western SEA, which includes Myanmar, with enhanced winds speed and reduced air temperature, implying increased rainfall. The anticyclonic pattern appeared to move to the BoB region strengthening the intensity of sub-tropical jets, pushing them further into continental land masses.

To assess the rainfall variability and its relationship with regional-scale atmospheric circulation, oceanic temperature, and monsoon indices, a composite analysis was performed. To do so, the regional-scale monthly and annual rainfall standardized index was developed to the inter-annual scale.

To further clarify the atmospheric circulation and its possible association with monsoon rainfall, we assessed the pressure vertical velocity (ω) for the wet and dry periods along latitude 15°, 20°, and 25° N, as shown in Figure 11. The results reveal that upward (rising) motions over the region were significant positive anomalies at 15° and 20° N (Figure 11a,c,e). Sinking motion occurred over the region during dry years, characterized by the significant positive anomaly at 15° and 20° N (Figure 11b,d,f). The difference in wet minus dry period moisture transport at 850 hPa revealed that anomalous moisture convergence (positive anomalies) emerge in the central and northern regions where moisture comes from BoB and the Gulf of Thailand (Figure S1). We also identified a relationship between the distribution of air space at lower and higher levels and the flow of moisture transport. An unfamiliar airfield at low levels aligned with the location of a large junction of the complete flow of moisture in a stormy area. Figure S2 shows the distribution of field streams for the diversity of summer varieties for wet drying seasons at 850 hPa. The cyclonic broadcast in Southern Myanmar during the period 1950–2019 occurred in the southwest, with its center around 10° N (Taninthary region). Therefore, more water vapor entered the region, especially since the convergence center of the corresponding humidity was associated with a clear climate zone that cuts the region, increasing rainfall in that region. In these cases, water vapor from the BoB and the Andaman Sea was transported into the land.

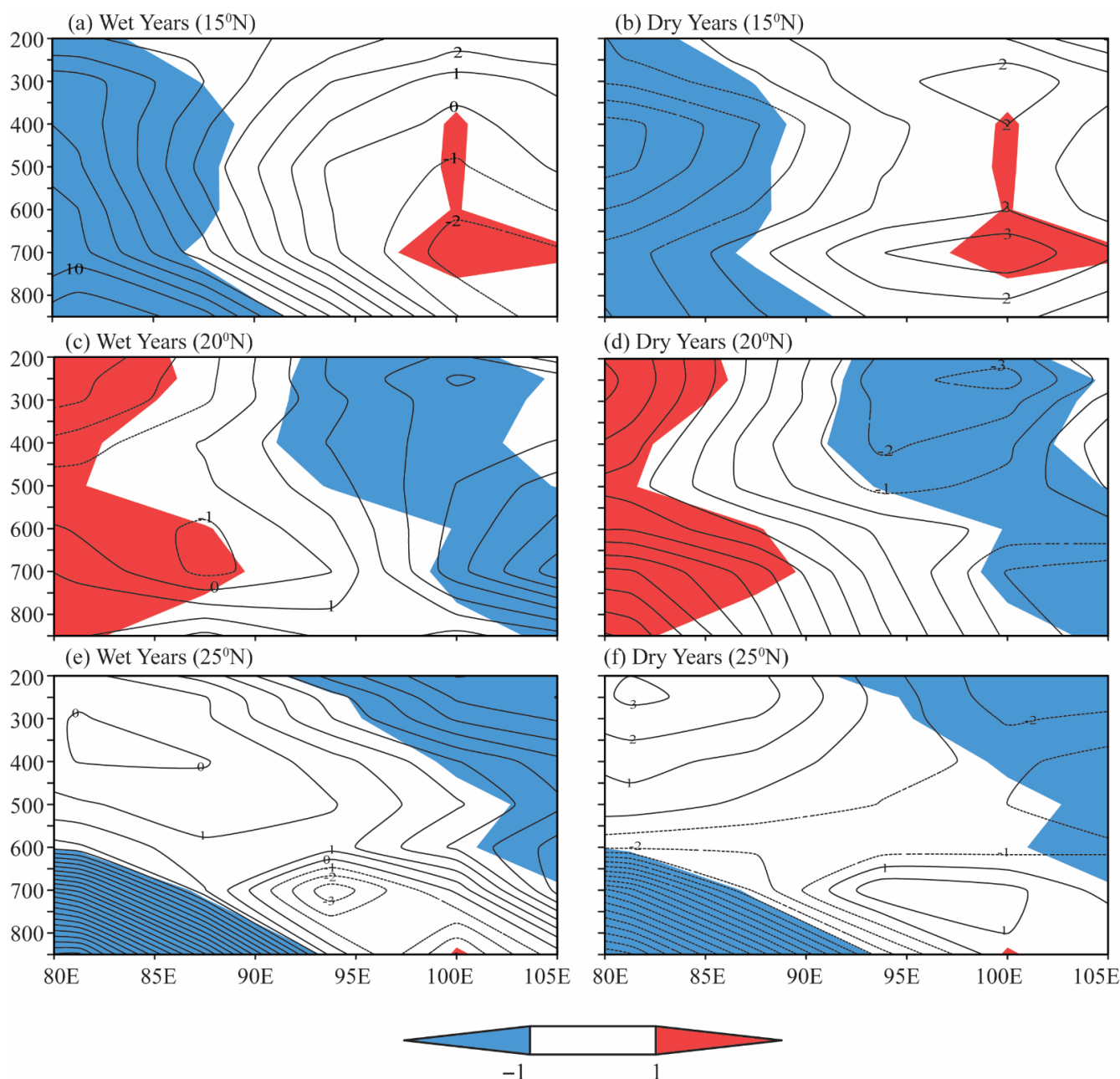


Figure 11. Pressure vertical velocity (ω) ($\times 10^{-3} \text{ Pa s}^{-1}$) over Myanmar during wet years (1962–1967, 1998, and 2003–2004) and dry years (1978–1986 and 1988–1990): (a) wet years at 15° N, (b) dry years at 15° N, (c) wet years at 20° N, (d) dry years at 20° N, (e) wet years at 25° N, and (f) dry years at 25° N. The red (blue) color indicates a positive (negative) significant anomaly. The dashed (solid) lines show ascending (descending) motion. Negative (positive) values indicate an upward (downward) motion.

4.3.3. Role of Oceans

From the composite analysis, we elucidated that large-scale atmospheric circulation had less (not-significant) influence on the summer monsoon rainfall variability over Myanmar. The observed relationship was rather weaker and could not be associated with rainfall variability over the study region. However, the composite analysis revealed that the anomalous wind pattern led the rainfall variability due to the regional rainfall dependence on moisture/water vapor. The trend in rainfall was obvious but the driver of the trend appeared to be complex; a simple mean trend may not provide enough explanation since sub-seasonal variability may balance each other, which may smooth or even remove the trend.

Figure 12 reveals a correlation map between the mean May–October SST (over the Indian Ocean and the Pacific Ocean) and mean May–October rainfall over Myanmar. A significant correlation (hatched regions) is displayed at the 95% confidence level in Figure 12. The results show a strong negative correlation between rainfall over Myanmar and Indian Ocean SST, which means that more (less) rainfall was recorded over Myanmar and with cooling (warming) over the Indian Ocean. The results further indicate that the air temperature in the northwest part of the SEA was obviously higher than in the southeast part of the region, which may affect the indicator of regional extreme temperature. Interestingly, we detected increasing trends in warm temperature events in the northern part of the region, in agreement with previous studies in the target regions [81,88]. Kreft and Eckstein (2013b) examined the monsoon rainfall over Myanmar and found a negative correlation with the positive phase of the Indian Ocean dipole (IOD).

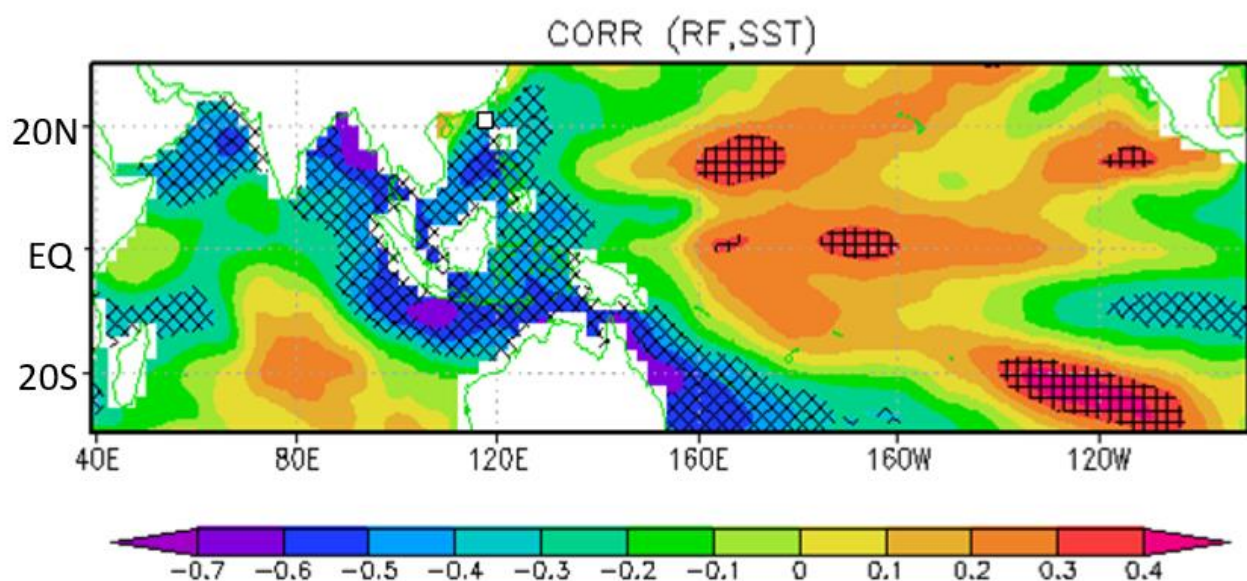


Figure 12. Correlation map between the mean decadal May–October SST (over the Indian Ocean and Pacific Ocean) and mean decadal May–October rainfall over Myanmar. Hatched regions show a significant correlation at the 95% confidence level.

This instability in the increase/decrease in SST and maximum/minimum rainfall may be associated with the increasing (decreasing) trend in temperature over the target region, which might affect the extreme temperature occurrences in the study area. The increase in frequency and magnitude of daily extreme warm temperature and decrease in extreme cold temperature may occur on the global scope, resulting in the increase in length, frequency, and/or intensity of warm periods or heat waves for most land areas [4,33]. Strong winds can transport water vapor from the ocean to nearby coastal areas, which can affect regional temperatures and ultimately affect the cooling trends, and vice versa [4,5].

The interdecadal variability in the 10 year running mean in Myanmar rainfall anomaly was computed using standardized deviation, PDO, and AMO indices, with the results provided in Figure 14. The effect of positive PDO was low rainfall (dry/drought), and that of negative PDO was more rainfall (wet/flood) in the region (Figure 14). The PDO index was statistically significant with a strong negative correlation with rainfall (−0.79), and the AMO index correlation coefficient explained the positive correlation (0.53), as shown in Table 4. The correlation coefficients between the Myanmar rainfall and various climate indices for the interannual and interdecadal components are presented in Table 4. The correlation coefficients between PDO and AMO indices and Myanmar rainfall for both the interannual and interdecadal components were significant at the 95% confidence level. The Myanmar rainfall showed a highly negative correlation with the PDO index and a positive correlation with the AMO index, particularly for the interdecadal component. The

cumulative role of these large-scale indices, especially during monsoon season, is perceived as affecting the SEA monsoon circulation pattern and thus resulting in dry/wet conditions during El Niño/La Niña years. The findings of the current study showed no obvious or significant association between ENSO, PDO, and monsoon onset timing with rainfall variability over Myanmar. The cold phase of the AMO is generally associated with negative Myanmar rainfall anomalies, which is lower than normal rainfall. The warming or positive phase PDO may decrease rainfall (drought) conditions, and cooling or negative-phase PDO may increase rainfall (flood) conditions over Myanmar. Moreover, there were nine extreme years (1952, 1959, 1961, 1965, 1970, 1973, 1974, 1999, and 2001), as shown in Figure 13. The results of extreme rainfall measures during the negative phases of the PDO show that no extreme events occurred during the positive phase of the PDO (Figure 13).

Various studies of linearly coupled dominating patterns between the global SST and rainfall variations in Myanmar related to the interdecadal variability have been conducted using the SVD method [4,31,37,81]. This method has successfully been applied in the region to identify the interannual variability in summer monsoon rainfall [89]. Figure 15 indicates the heterogeneous correlation of the first three SVD modes amongst global SST and Myanmar rainfall. The SVD of the SST modes closely represents the long-term global warming pattern (Figure 15a,e), with a correlation coefficient of 0.94 between the time series of its principal components and the low-pass-filtered global SST anomaly. The southern and eastern regions of Myanmar and regions of the mid-west extending up to Indian Ocean are strongly correlated with SST in the tropical and northern Pacific (Figure 15a,b). We found subtle differences in the global spatial structure of the tropical Pacific SST correlation pattern in this period (Figure 15c). Although it is unclear if the differences in the global SST spatial patterns for the three modes regional rainfall are statistically significant, they do provide some insights. The findings reported using heterogeneous correlation patterns [11] as the first SVD of SST mode 1 were mainly associated with the cold phase of PDO in the Pacific Ocean, north of 20° N, and the warm phase of AMO in the North Atlantic Ocean (Figure 15a). The rainfall mode 1 explains much of the rainfall over the regions except for the central core and eastern regions (Figure 15b). The squared covariance fraction of this mode is about 53%, and the correlation coefficient between the two fields is 0.94. SVD2 of SST mode 2 demonstrated a warm SST in the eastern equatorial Pacific SST, like the El Niño SST pattern in the Pacific Ocean, and a cold SST in the North Atlantic Ocean (Figure 15c). The result show that relatively low rainfall over the region contributed to rainfall mode 2 (Figure 15d). Thus, the El Niño SST pattern in the Pacific Ocean and cold phase of the AMO were associated with dry/drought conditions over the region. The time series of the coefficients for the three SVD modes of global ocean SST and Myanmar rainfall are presented in Figure 16. The squared covariance fraction of SVD mode 2 was detected at a rate of 33%, and the correlation coefficient between the two fields' time coefficients is around 0.94. SST mode 3 explains cold SSTs in the central and eastern equatorial Pacific SSTs as a La Niña SST pattern (Figure 15e). Rainfall mode 3 exhibits enhanced rainfall over the region (Figure 15f). SVD3 of the squared covariance fraction of this mode was detected with a 6.7% rate, and the correlation coefficient between the two fields is 0.93 (Table 5). Therefore, we inferred that the role of the oceanic circulation is important for decadal Myanmar rainfall.

Table 4. Correlation coefficients between various indices and Myanmar rainfall for interannual and interdecadal components. * Significant values at the 95% confidence level. NP, North Pacific index; NAO, North Atlantic oscillation index; AO, Arctic oscillation.

Indices	Interannual Component	Interdecadal Component
NP	−0.24	−0.17
NAO	−0.38 *	−0.15
AO	−0.02	−0.21
PDO	−0.39 *	−0.79 *
AMO	0.53 *	0.54 *

Table 5. Statistics of the leading singular value decomposition (SVD) sea surface temperature (SST) and rainfall modes over the study area.

Mode	Squared Covariance	Temporal Correlation	SST Variance	Rainfall Variance
Mode 1	53%	0.94	47%	20%
Mode 2	33%	0.94	21%	28%
Mode 3	6.7%	0.93	9%	13%

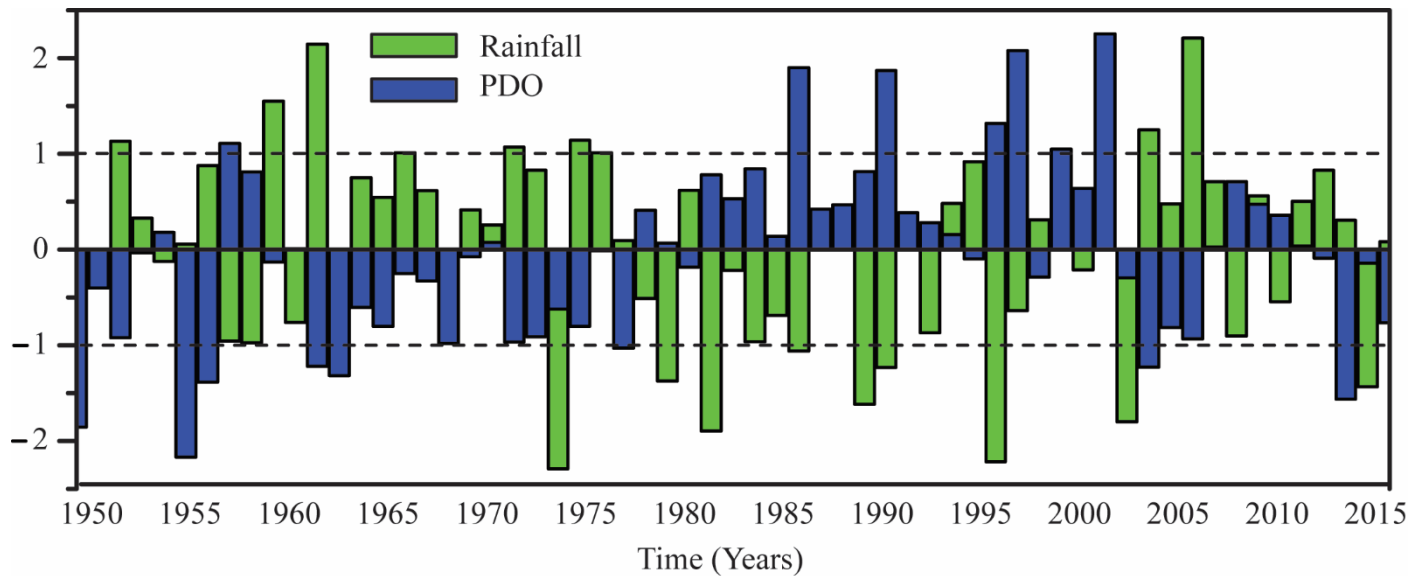


Figure 13. Time series of the normalized summer monsoon rainfall in Myanmar (1950–2010). The blue bars indicate the multidecadal variability (MDV) in the PDO index obtained using the ensemble empirical mode decomposition (EEMD) method.

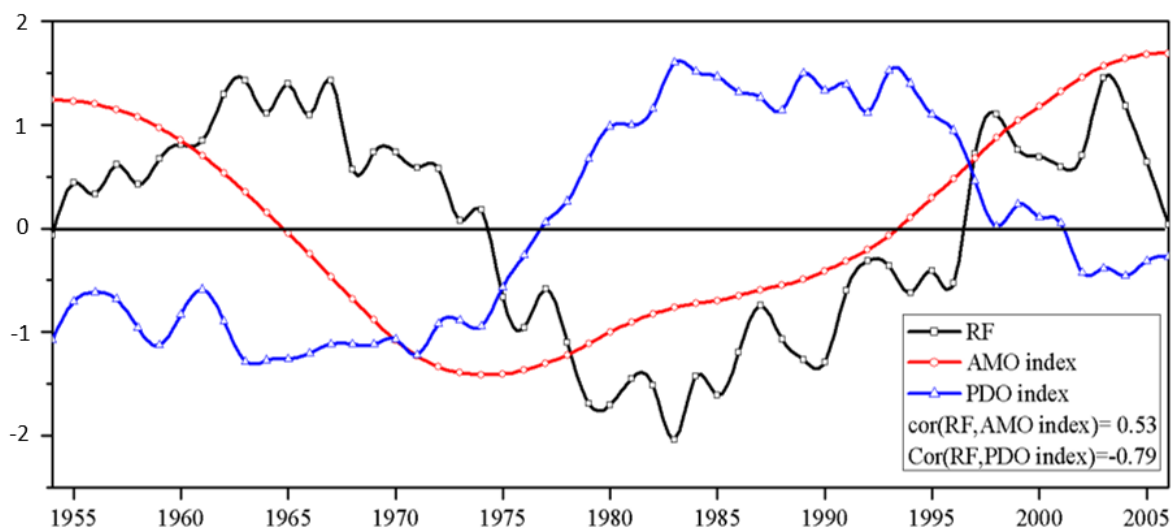


Figure 14. Interdecadal variability in average 10 year running mean summer monsoon rainfall anomaly based on standard deviation, Pacific decadal oscillation (PDO), and Atlantic multidecadal oscillation (AMO) indices.

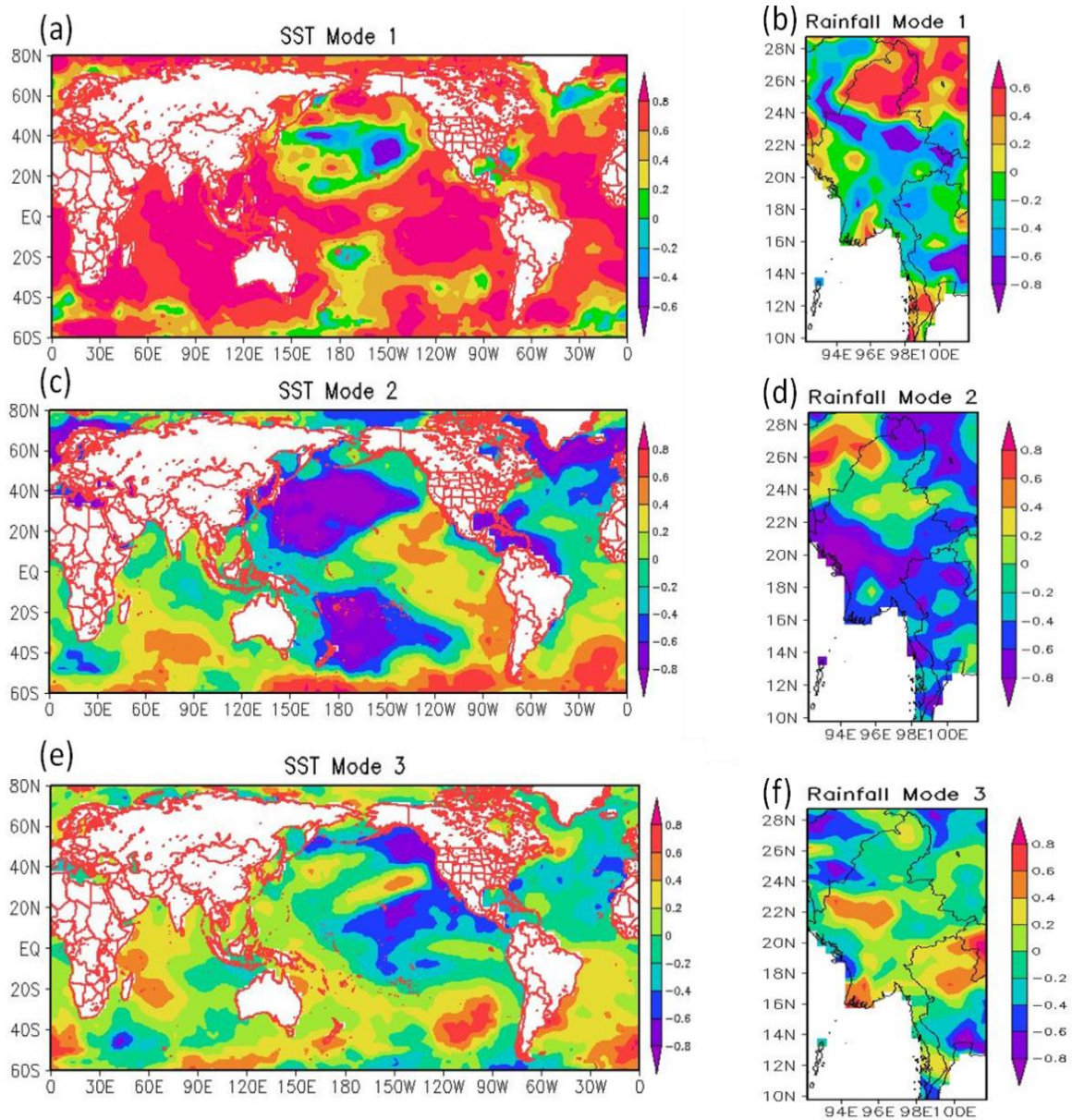


Figure 15. Heterogeneous correlations of the first three SVD modes among global SST and Myanmar rainfall: (a) SST mode 1, (b) rainfall mode 1, (c) SST mode 2, (d) rainfall mode 2, (e) SST mode 3, and (f) rainfall mode 3.

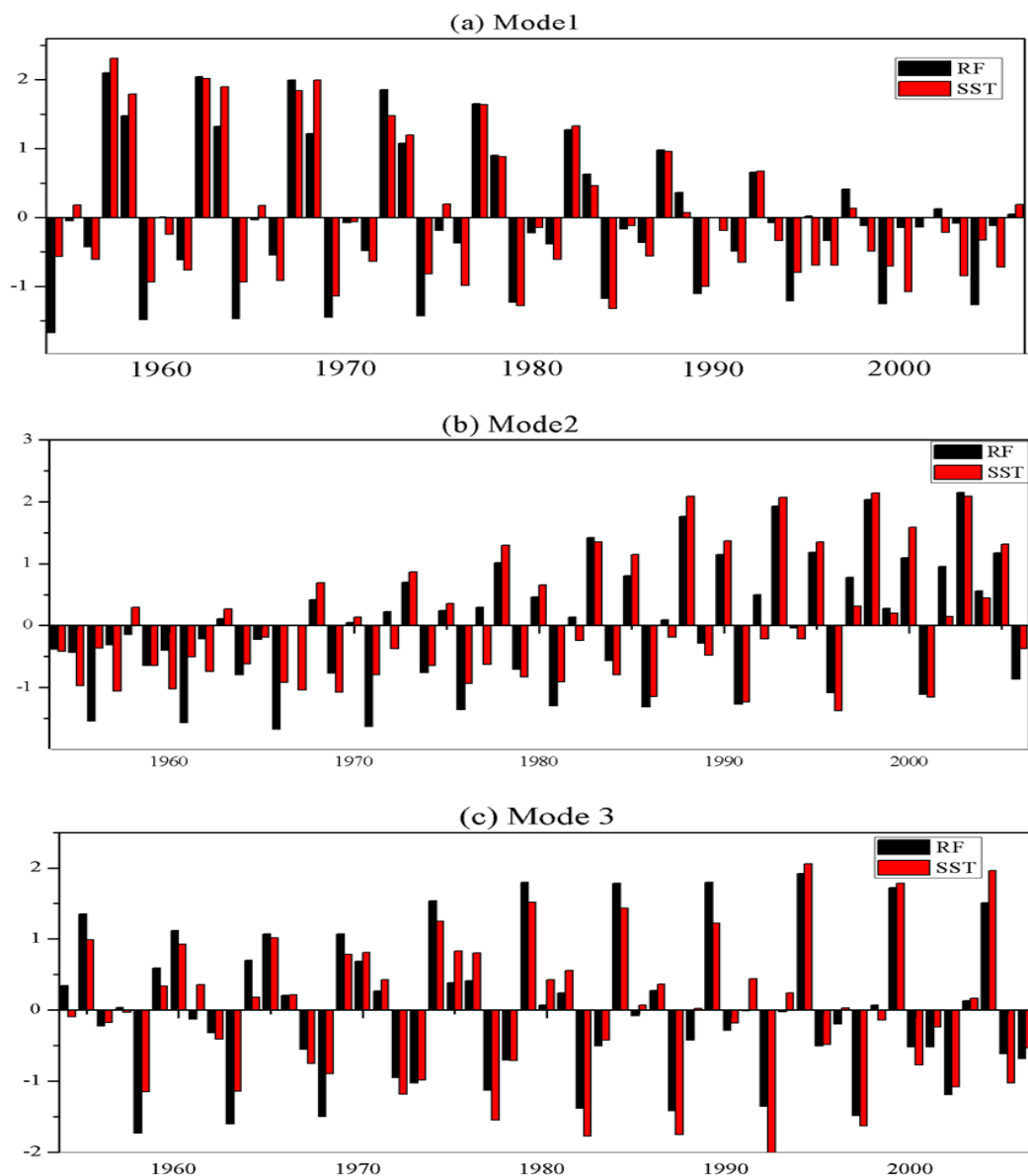


Figure 16. Normalized time series of the first three SVD modes: (a) mode 1, (b) mode 2, and (c) mode 3 SST (red bars) and rainfall (black bars).

5. Discussion

In this study, we evaluated the interdecadal variability in the summer monsoon rainfall (May–October) in Myanmar (1950–2019) using EOF, SVD, EEMD, and correlation analyses based on 10 year running means. This study is the first of its kind to use a large number of statistical approaches to investigate the interdecadal variability in monsoon rainfall, which is beneficial for the scientific community and climate change adaptation in Myanmar. The results reveal that the dominant summer monsoon regions (south, central, and east) observed dry conditions during 1998 and 2002. Sein et al., (2015) described the lowest rainfall over Myanmar since 1997, and the most intensive heat wave (60%) occurred in 1998 during an ENSO year. Webster and Yang (1992) [90] showed that 1998 was the driest year during the period of 1950–2019, with extreme temperature recorded in May 1998 (43.6 °C). Our results agree with the findings of previous studies [27], reporting similar results over the target regions. We used EOF analysis with the 10 year running means of summer monsoon rainfall, and the results show that the first leading EOF pattern explained 47% of the variance. The maximum loading occurs along the western coast and the minimum

in the northwest region, while the corresponding PC1 exhibits a dipole pattern. Our results support the findings of Zhang et al., (2014), who reported similar results over South China using a drought index. The circulation patterns on an interdecadal scale 2343 analyzed using the composites (dry and wet years) in this study. Interdecadal variability in circulation mode consists of upward (rising) motion over the region, significantly positive anomaly over central Myanmar. The southwest moisture flux comes from the north Indian Ocean across the entire west coast of Myanmar.

Reckien and Petkova (2019) [91] studied the first component of EOF of the vertically integrated moisture transport vector in summer, and strong northward moisture transport from the tropical Indian and West Pacific Oceans dominated the whole East Asian region. In this study, PDO index values were found to be significantly related to Myanmar summer monsoon rainfall (-0.79) during the 1950–2019 period. The result show a positive correlation with phase changes in the PDO, but negative PDO change was found with lower summer monsoon rainfall over Myanmar, which agrees with Roy et al., (2011) and Kumar et al., (2006). Lone et al., (2019) investigated the ENSO, PDO, and the summer monsoon rainfall in Myanmar over 52 years (1951–2002). They found that the overall negative relationship between ENSO and rainfall patterns had a strong positive association across Myanmar. The role of ENSO in the resulting rainfall patterns during El Niño years was stronger during the cold phase of the PDO compared with during La Niña years. The difference between rainfall during the different phases of ENSO was superimposed with the warm and cold periods of the PDO, showing overall higher average annual rainfall during cold PDO episodes [92].

The results reveal that the Indian monsoon is more vulnerable to drought when El Niño events occur during warm phases of the Pacific interdecadal variability. Conversely, wet monsoons are more likely to prevail when La Niña events coincide during cold phases of the Pacific interdecadal variability. Based on the EEMD analysis, highly extreme summer monsoon rainfall (i.e., 1952, 1959, 1961, 1965, 1970, 1973, 1974, 1999, and 2001) occurs during the negative phases of the PDO; no extreme events occurred during the positive phase of the PDO. Our results support the findings of Chen and Huang (2017), who described that between 1951 and 2012, there were five extreme events that had a strong correlation with the negative phases of the PDO. The AMO index was significantly associated with Myanmar summer monsoon rainfall recorded, at 0.54. Here, to determine the interdecadal summer monsoon rainfall modes and SST, a further SVD analysis was performed. The results of SVD mode 1 explain that the positive phase of the AMO receives higher summer monsoon rainfall, except in central and east regions in Myanmar. The positive phase of the AMO significantly correlated with higher summer monsoon rainfall and negatively correlated with lower summer monsoon rainfall over Myanmar, which is in agreement with Sein et al., (2015).

Our findings do not negate the potential impact of large-scale oceanic indices but rather postulate the hypothesis that these controls need to be reviewed with clear links to summer monsoon rainfall variability over Myanmar. Another possible reason could be the quality of station data, since they are recorded for synoptic-scale use and climatological processes usually occur on longer time scale; thus, the data may lack such large-scale signals. These are some of the points that need to be thoroughly investigated in future studies, including the frequency and intensity of extreme rainfall events and their role as drivers of regional rainfall variability.

6. Conclusions

In this study, we attempted to explore the spatiotemporal trend and variability in monsoon rainfall during the period of 1950–2019 over Myanmar. Using statistical and composite analyses, we found significant variation in rainfall on seasonal, annual, and interdecadal scales. The main conclusions based on the findings are as follows:

- (1) The interdecadal variation over the target region increased in the late 1950s, reaching its peak around 1965, and subsequently decreased in the mid-1980s before increasing again in the early 1990s. An abrupt rainfall shift was recorded during the 1970s and a significant reduction (at the 95% confidence level) in rainfall was evident between the 1980s and the 2000s.
- (2) In terms of rainfall trend, the regional variability in monsoon rainfall over Myanmar was obvious during the 1950–2019 period. The magnitude of the rainfall variability could possibly be associated with the geographical location of the region and monsoon circulation patterns. The temporal trend over the Asian and Indian monsoon systems showed strong variation on different time scales, including monthly, inter-annual, intra-seasonal, and annual time scales. Such large-scale variation caused by different factors could induce changes in monsoon rainfall over the diverse study regions.
- (3) The widely used EOF method showed that the interdecadal rainfall pattern over Myanmar significantly changed over the study period, especially during EOF2 and EOF3. PC1 and PC2 experienced an increasing trend over the target region during the period 1950–2019.
- (4) The results further demonstrate the significant negative westerly and southwesterly wind anomalies from the BoB and Andaman Sea over almost the whole region except for the eastern and southern regions during wet years. The moisture transport at 850 hPa revealed that the anomalous moisture convergence (positive anomalies) emerged in the central and northern region, transporting moisture from the Western BoB and Eastern Gulf of Thailand. This cyclonic circulation may cause more water vapor from the BoB and Andaman Sea to be transported into the country. In addition, warm or positive PDO phase was associated with low rainfall in Myanmar, and cooling or negative PDO phase can increase rainfall over Myanmar. The AMO index had a mean average value of 0.53 for the same period. In addition, the effects of excessive rainfall occurred in the negative stages of the PDO, and no serious adverse events occurred in the positive phase of the PDO. The first SVD of SST mode 1 was mainly linked to the PDO cold phase in the Pacific Ocean above the North Pacific Ocean (20° N) and the warm AMO phase in the North Atlantic Ocean.
- (5) The SST patterns showed that the warm SST of the eastern equatorial Pacific SST is a pattern of the El Niño SST in the Pacific Ocean and the cold SST in the North Atlantic Ocean. The fractional covariance fraction of SVD2 was recorded as 33%, whereas the coefficient of correlation between the coefficients for the two-phase period was 0.94. Therefore, we concluded that the findings of the present study provide valuable results regarding the interdecadal variability in Myanmar summer monsoon rainfall, which is shown as a negative correlation with the PDO and a positive association with the AMO. In addition, Myanmar's decadal summer monsoon rainfall and relationships with the PDO and AMO indexes explain the flood and dry conditions (drought) in the region.

Supplementary Materials: The following are available online at <https://www.mdpi.com/2073-4441/13/5/729/s1>, Figure S1: Difference fields of wet period (1962–1967, 1998, 2003–2004) minus dry period (1978–1986, 1988–1990) of moisture transport at 850 hPa ($\text{g kg}^{-1} \text{ms}^{-1}$) over Myanmar computed from ERA-interim dataset. Vector shows moisture transport, while the shaded regions specify convergence (positive) and divergence (negative) moisture fluxes convergence., Figure S2: Difference stream fields of wet period (1962–1967, 1998, 2003–2004) minus dry period (1978–1986, 1988–1990) at 850 hPa in summer.

Author Contributions: Conceptualization, Z.M.M.S., I.U., and X.Z.; Methodology, Software, and Validation, Z.M.M.S. and X.Z.; Formal Analysis and Investigation, I.U. and Z.M.M.S.; Writing—Review and Editing, I.U., F.S. and S.S.; Data curation, K.A., S.S. and Z.M.M.S. All authors have read and agreed to the published version of the manuscript.

Funding: This study supported by the National (Key) Basic R&D Program of China (grant no. 2012CB955204).

Institutional Review Board Statement: Not applicable.

Informed Consent Statement: Not Applicable.

Data Availability Statement: Not Applicable.

Acknowledgments: We thank the two anonymous reviewers for their time and support in re-shaping the manuscript. Their comments helped us to improve the final version of the manuscript. This research was encouraged by Binjiang College, Nanjing University of Information Science and Technology, Wuxi City, Jiangsu Province, China. Special appreciation to the Department of Meteorology and Hydrology, Myanmar, for the provision of the datasets used in the study.

Conflicts of Interest: The authors declare no conflict of interest.

References

- Goswami, B.N.; Madhusoodanan, M.S.; Neema, C.P.; Sengupta, D. A physical mechanism for North Atlantic SST influence on the Indian summer monsoon. *Geophys. Res. Lett.* **2006**, *33*. [[CrossRef](#)]
- Saleem, F.; Zeng, X.; Hina, S.; Omer, A. Regional changes in extreme temperature records over Pakistan and their relation to Pacific variability. *Atmos. Res.* **2021**, *250*, 105407. [[CrossRef](#)]
- Hina, S.; Saleem, F. Historical analysis (1981–2017) of drought severity and magnitude over a predominantly arid region of Pakistan. *Clim. Res.* **2019**, *78*, 189–204. [[CrossRef](#)]
- Suman, M.; Maity, R. Southward shift of precipitation extremes over south Asia: Evidences from CORDEX data. *Sci. Rep.* **2020**, *10*, 1–11. [[CrossRef](#)]
- Ren, Y.-Y.; Ren, G.-Y.; Sun, X.-B.; Shrestha, A.B.; You, Q.-L.; Zhan, Y.-J.; Rajbhandari, R.; Zhang, P.-F.; Wen, K.-M. Observed changes in surface air temperature and precipitation in the Hindu Kush Himalayan region over the last 100-plus years. *Adv. Clim. Chang. Res.* **2017**, *8*, 148–156. [[CrossRef](#)]
- Lone, S.A.; Jeelani, G.; Deshpande, R.D.; Mukherjee, A. Stable isotope ($\delta^{18}\text{O}$ and δD) dynamics of precipitation in a high altitude Himalayan cold desert and its surroundings in Indus river basin, Ladakh. *Atmos. Res.* **2019**, *221*, 46–57. [[CrossRef](#)]
- Zhi, X.; Tian, X.; Liu, P.; Hu, Y. Interdecadal variations in winter extratropical anticyclones in East Asia and their impacts on the decadal mode of East Asian surface air temperature. *Theor. Appl. Clim.* **2019**, *131*, 1763–1775. [[CrossRef](#)]
- Hou, M.; Duan, W.; Zhi, X. Season-dependent predictability barrier for two types of El Niño revealed by an approach to data analysis for predictability. *Clim. Dyn.* **2019**, *53*, 5561–5581. [[CrossRef](#)]
- Tangang, F.; Chung, J.X.; Juneng, L.; Supari, Salimun, E.; Ngai, S.T.; Jamaluddin, A.F.; Mohd, M.S.F.; Cruz, F.; Narisma, G.; et al. Projected future changes in rainfall in Southeast Asia based on CORDEX–SEA multi-model simulations. *Clim. Dyn.* **2020**, *55*, 1247–1267. [[CrossRef](#)]
- Almazroui, M.; Saeed, S.; Saeed, F.; Islam, M.N.; Ismail, M. Projections of Precipitation and Temperature over the South Asian Countries in CMIP6. *Earth Syst. Environ.* **2020**, *4*, 297–320. [[CrossRef](#)]
- Ge, F.; Zhu, S.; Luo, H.; Zhi, X.; Wang, H. Future changes in precipitation extremes over Southeast Asia: Insights from CMIP6 multi-model ensemble. *Environ. Res. Lett.* **2021**, *16*, 024013. [[CrossRef](#)]
- Song, B.; Zhi, X.; Pan, M.; Hou, M.; He, C.; Fraedrich, K. Turbulent Heat Flux Reconstruction in the North Pacific from 1921 to 2014. *J. Meteorol. Soc. Jpn.* **2019**, *97*, 893–911. [[CrossRef](#)]
- Francis, R.C.; Hare, S.R. Decadal-scale regime shifts in the large marine ecosystems of the North-east Pacific: A case for historical science. *Fish. Oceanogr.* **1994**, *3*, 279–291. [[CrossRef](#)]
- Latif, M.; Barnett, T.P. Causes of Decadal Climate Variability over the North Pacific and North America. *Science* **1994**, *266*, 634–637. [[CrossRef](#)]
- Yang, Y.; Gan, T.Y.; Tan, X. Spatiotemporal Changes in Precipitation Extremes over Canada and Their Teleconnections to Large-Scale Climate Patterns. *J. Hydrometeorol.* **2019**, *20*, 275–296. [[CrossRef](#)]
- Ge, F.; Zhu, S.; Peng, T.; Zhao, Y.; Sielmann, F.; Fraedrich, K.; Zhi, X.; Liu, X.; Tang, W.; Ji, L. Risks of precipitation extremes over Southeast Asia: Does 1.5 °C or 2 °C global warming make a difference? *Environ. Res. Lett.* **2019**, *14*, 044015. [[CrossRef](#)]
- Ge, F.; Zhi, X.; Babar, Z.A.; Tang, W.; Chen, P. Interannual variability of summer monsoon precipitation over the Indochina Peninsula in association with ENSO. *Theor. Appl. Clim.* **2016**, *128*, 523–531. [[CrossRef](#)]
- Liu, B.; Wu, G.; Ren, R. Influences of ENSO on the vertical coupling of atmospheric circulation during the onset of South Asian summer monsoon. *Clim. Dyn.* **2014**, *45*, 1859–1875. [[CrossRef](#)]
- Xu, J.; Koldunov, N.V.; Remedio, A.R.C.; Sein, D.V.; Rechid, D.; Zhi, X.; Jiang, X.; Xu, M.; Zhu, X.; Fraedrich, K.; et al. Downstream effect of Hengduan Mountains on East China in the REMO regional climate model. *Theor. Appl. Clim.* **2018**, *135*, 1641–1658. [[CrossRef](#)]
- Zhang, L.; Zhu, X.; Fraedrich, K.; Sielmann, F.; Zhi, X. Interdecadal variability of winter precipitation in Southeast China. *Clim. Dyn.* **2014**, *43*, 2239–2248. [[CrossRef](#)]
- Zheng, Y.; Zhang, Q.; Luo, M.; Sun, P.; Singh, V.P. Wintertime precipitation in eastern China and relation to the Madden-Julian oscillation: Spatiotemporal properties, impacts and causes. *J. Hydrol.* **2020**, *582*, 124477. [[CrossRef](#)]

22. Mantua, N.J.; Hare, S.R.; Zhang, Y.; Wallace, J.M.; Francis, R.C. A Pacific Interdecadal Climate Oscillation with Impacts on Salmon Production. *Bull. Am. Meteorol. Soc.* **1997**, *1069–1079*. [[CrossRef](#)]
23. Zhang, L.; Sielmann, F.; Fraedrich, K.; Zhu, X.; Zhi, X. Variability of winter extreme precipitation in Southeast China: Contributions of SST anomalies. *Clim. Dyn.* **2015**, *45*, 2557–2570. [[CrossRef](#)]
24. Chhin, R.; Shwe, M.M.; Yoden, S. Time-lagged correlations associated with interannual variations of pre-monsoon and post-monsoon precipitation in Myanmar and the Indochina Peninsula. *Int. J. Clim.* **2020**, *40*, 3792–3812. [[CrossRef](#)]
25. Sein, Z.M.M.; Islam, A.R.M.T.; Maw, K.W.; Moya, T.B. Characterization of southwest monsoon onset over Myanmar. *Theor. Appl. Clim.* **2015**, *127*, 587–603. [[CrossRef](#)]
26. Burki, T. Floods in Myanmar damage hundreds of health facilities. *Lancet* **2015**, *386*, 843. [[CrossRef](#)]
27. Chen, F.-H.; Huang, W. Multi-scale climate variations in the arid Central Asia. *Adv. Clim. Chang. Res.* **2017**, *8*, 1–2. [[CrossRef](#)]
28. Zaw, Z.; Fan, Z.-X.; Bräuning, A.; Liu, W.; Gaire, N.P.; Than, K.Z.; Panthi, S. Monsoon precipitation variations in Myanmar since AD 1770: Linkage to tropical ocean-atmospheric circulations. *Clim. Dyn.* **2021**, 1–16. [[CrossRef](#)]
29. Ge, F.; Peng, T.; Fraedrich, K.; Sielmann, F.; Zhu, X.; Zhi, X.; Liu, X.; Tang, W.; Zhao, P. Assessment of trends and variability in surface air temperature on multiple high-resolution datasets over the Indochina Peninsula. *Theor. Appl. Clim.* **2019**, *135*, 1609–1627. [[CrossRef](#)]
30. Xu, J.; Koldunov, N.; Remedio, A.R.C.; Sein, D.V.; Zhi, X.; Jiang, X.; Xu, M.; Zhu, X.; Fraedrich, K.; Jacob, D. On the role of horizontal resolution over the Tibetan Plateau in the REMO regional climate model. *Clim. Dyn.* **2018**, *51*, 4525–4542. [[CrossRef](#)]
31. Kreft, S.; Eckstein, D. Global Climate Risk Index 2014: Who suffers most from extreme weather events? Weather-related loss events in 2012 and 1993 to 2012. *Ger. Brief. Pap.* **2013**, *28*.
32. Zhang, L.; Sielmann, F.; Fraedrich, K.; Zhi, X. Atmospheric response to Indian Ocean Dipole forcing: Changes of Southeast China winter precipitation under global warming. *Clim. Dyn.* **2016**, *48*, 1467–1482. [[CrossRef](#)]
33. Sen Roy, N.; Kaur, S. Climatology of monsoon rains of Myanmar (Burma). *Int. J. Climatol.* **2000**, 913–928. [[CrossRef](#)]
34. Zaw, Z.; Fan, Z.; Bräuning, A.; Xu, C.; Liu, W.; Gaire, N.P.; Panthi, S.; Than, K.Z. Drought Reconstruction Over the Past Two Centuries in Southern Myanmar Using Teak Tree-Rings: Linkages to the Pacific and Indian Oceans. *Geophys. Res. Lett.* **2020**, *47*. [[CrossRef](#)]
35. Zhang, L.; Zhi, X.F. Multimodel consensus forecasting of low temperature and icy weather over central and Southern China in early 2008. *J. Trop. Meteorol.* **2015**, 67–75. [[CrossRef](#)]
36. Sein, M.M.Z.; Ogwang, B.A.; Ongoma, V.; Ogou, F.K.; Batebana, K. Inter-annual variability of Summer Monsoon Rainfall over Myanmar in relation to IOD and ENSO. *J. Environ. Agric. Sci.* **2015**, *4*, 28–36.
37. Oo, S.S.; Hmwe, K.M.; Aung, N.N.; Su, A.A.; Soe, K.K.; Mon, T.L.; Lwin, K.M.; Thu, M.M.; Soe, T.T.; Htwe, M.L. Diversity of Insect Pest and Predator Species in Monsoon and Summer Rice Fields of Taungoo Environs, Myanmar. *Adv. Entomol.* **2020**, *8*, 117–129. [[CrossRef](#)]
38. Omer, A.; Elagib, N.A.; Zhuguo, M.; Saleem, F.; Mohammed, A. Water scarcity in the Yellow River Basin under future climate change and human activities. *Sci. Total. Environ.* **2020**, *749*, 141446. [[CrossRef](#)]
39. Schneider, U.; Becker, A.; Finger, P.; Meyer-Christoffer, A.; Ziese, M.; Rudolf, B. GPCC's new land surface precipitation climatology based on quality-controlled in situ data and its role in quantifying the global water cycle. *Theor. Appl. Clim.* **2014**, *115*, 15–40. [[CrossRef](#)]
40. Aadhar, S.; Mishra, V. A substantial rise in the area and population affected by dryness in South Asia under 1.5 °C, 2.0 °C and 2.5 °C warmer worlds. *Environ. Res. Lett.* **2019**, *14*, 114021. [[CrossRef](#)]
41. Ahmed, K.; Shahid, S.; Sachindra, D.; Nawaz, N.; Chung, E.-S. Fidelity assessment of general circulation model simulated precipitation and temperature over Pakistan using a feature selection method. *J. Hydrol.* **2019**, *573*, 281–298. [[CrossRef](#)]
42. Onyutha, C. Analyses of rainfall extremes in East Africa based on observations from rain gauges and climate change simulations by CORDEX RCMs. *Clim. Dyn.* **2020**, *54*, 4841–4864. [[CrossRef](#)]
43. Liu, Y.B.; Song, P.; Peng, J.; Fu, Q.N.; Dou, C.C. Recent increased frequency of drought events in Poyang Lake Basin, China: Climate change or anthropogenic effects? *Hydro-Climatol. Var. Chang.* **2011**, *344*, 99–104.
44. Khan, N.; Sachindra, D.; Shahid, S.; Ahmed, K.; Shiru, M.S.; Nawaz, N. Prediction of droughts over Pakistan using machine learning algorithms. *Adv. Water Resour.* **2020**, *139*, 103562. [[CrossRef](#)]
45. Zhang, T.; Lin, X. Assessing future drought impacts on yields based on historical irrigation reaction to drought for four major crops in Kansas. *Sci. Total. Environ.* **2016**, *550*, 851–860. [[CrossRef](#)]
46. Knight, J.H.; Minasny, B.; McBratney, A.B.; Koen, T.B.; Murphy, B.W. Soil temperature increase in eastern Australia for the past 50 years. *Geoderma* **2018**, *313*, 241–249. [[CrossRef](#)]
47. Rayner, N.A.; Parker, D.E.; Horton, E.B.; Folland, C.K.; Alexander, L.V.; Rowell, D.P.; Kent, E.C.; Kaplan, A.L. Global analyses of sea surface temperature, sea ice, and night marine air temperature since the late nineteenth century. *J. Geophys. Res. Space Phys.* **2003**, *108*. [[CrossRef](#)]
48. Hersbach, H.; Bell, B.; Berrisford, P.; Horányi, A.; Sabater, J.M.; Nicolas, J.; Radu, R.; Schepers, D.; Simmons, A.; Soci, C.; et al. Global reanalysis: Goodbye ERA-Interim, hello ERA5. *ECMWF Newsl.* **2019**, 17–24. [[CrossRef](#)]
49. Hersbach, H.; Bell, B.; Berrisford, P.; Hirahara, S.; Horányi, A.; Muñoz-Sabater, J.; Nicolas, J.; Peubey, C.; Radu, R.; Schepers, D.; et al. The ERA5 global reanalysis. *Q. J. R. Meteorol. Soc.* **2020**, *146*, 1999–2049. [[CrossRef](#)]

50. Smith, T.M.; Reynolds, R.W.; Peterson, T.C.; Lawrimore, J. Improvements to NOAA's Historical Merged Land–Ocean Surface Temperature Analysis (1880–2006). *J. Clim.* **2008**, *21*, 2283–2296. [[CrossRef](#)]
51. Kalnay, E.; Kanamitsu, M.; Kistler, R.; Collins, W.; Deaven, D.; Gandin, L.; Iredell, M.; Saha, S.; White, G.; Woollen, J.; et al. The NCEP/NCAR 40-year reanalysis project. *Bull. Am. Meteorol. Soc.* **1996**, *37*–472. [[CrossRef](#)]
52. Mardia, K.V. Multi-dimensional multivariate Gaussian Markov random fields with application to image processing. *J. Multivar. Anal.* **1988**, *24*, 265–284. [[CrossRef](#)]
53. Hannachi, A.; Jolliffe, I.T.; Stephenson, D.B. Empirical orthogonal functions and related techniques in atmospheric science: A review. *Int. J. Clim.* **2007**, *27*, 1119–1152. [[CrossRef](#)]
54. Levine, R.A.; Wilks, D.S. Statistical Methods in the Atmospheric Sciences. *J. Am. Stat. Assoc.* **2000**, *95*, 344. [[CrossRef](#)]
55. Walsh, J.E.; Mostek, A. A Quantitative Analysis of Meteorological Anomaly Patterns Over the United States, 1900–1977. *Mon. Weather. Rev.* **1980**, *108*, 615–630. [[CrossRef](#)]
56. Smakhtin, V.U.; Hughes, D.A. Automated estimation and analyses of meteorological drought characteristics from monthly rainfall data. *Environ. Model. Softw.* **2007**, *22*, 880–890. [[CrossRef](#)]
57. Gilman, D.L.; Fuglister, F.J.; Mitchell, J.M. On the Power Spectrum of “Red Noise”. *J. Atmos. Sci.* **1963**, 182–184. [[CrossRef](#)]
58. Mitchell, J.M. Further Remarks on the Power Spectrum of “Red Noise”. *J. Atmos. Sci.* **1964**, 461. [[CrossRef](#)]
59. Joshi, M.K.; Pandey, A.C. Trend and spectral analysis of rainfall over India during 1901–2000. *J. Geophys. Res. Space Phys.* **2011**, *116*. [[CrossRef](#)]
60. Zhu, S.; Ge, F.; Fan, Y.; Zhang, L.; Sielmann, F.; Fraedrich, K.; Zhi, X. Conspicuous temperature extremes over Southeast Asia: Seasonal variations under 1.5 °C and 2 °C global warming. *Clim. Chang.* **2020**, *160*, 343–360. [[CrossRef](#)]
61. Folland, C.K.; Knight, J.; Linderholm, H.W.; Fereday, D.; Ineson, S.; Hurrell, J.W. The Summer North Atlantic Oscillation: Past, Present, and Future. *J. Clim.* **2009**, *22*, 1082–1103. [[CrossRef](#)]
62. Wen, Z.; Niu, F.; Yu, Q.; Wang, D.; Feng, W.; Zheng, J. The role of rainfall in the thermal-moisture dynamics of the active layer at Beiluhe of Qinghai-Tibetan plateau. *Environ. Earth Sci.* **2013**, *71*, 1195–1204. [[CrossRef](#)]
63. Banacos, P.C.; Schultz, D.M. The Use of Moisture Flux Convergence in Forecasting Convective Initiation: Historical and Operational Perspectives. *Weather Forecast.* **2005**, *20*, 351–366. [[CrossRef](#)]
64. Mann, H.B. Nonparametric Tests against Trend. *Econometrica* **1945**, *13*, 245. [[CrossRef](#)]
65. Kendall, M.G. *Rank Correlation Methods*; Griffin: London, UK, 1975; ISBN 0852641990.
66. Ghosh, K.G. Spatial and temporal appraisal of drought jeopardy over the Gangetic West Bengal, eastern India. *Geoenvironmental Disasters* **2019**, *6*, 1. [[CrossRef](#)]
67. Waseem, M.; Ahmad, I.; Mujtaba, A.; Tayyab, M.; Si, C.; Lü, H.; Dong, X. Spatiotemporal Dynamics of Precipitation in Southwest Arid-Agriculture Zones of Pakistan. *Sustainability* **2020**, *12*, 2305. [[CrossRef](#)]
68. Payab, A.H.; Türker, U. Comparison of standardized meteorological indices for drought monitoring at northern part of Cyprus. *Environ. Earth Sci.* **2019**, *78*, 309. [[CrossRef](#)]
69. Naz, F.; Dars, G.H.; Ansari, K.; Jamro, S.; Krakauer, N.Y. Drought Trends in Balochistan. *Water* **2020**, *12*, 470. [[CrossRef](#)]
70. Musonda, B.; Jing, Y.; Iyakaremye, V.; Ojara, M. Analysis of Long-Term Variations of Drought Characteristics Using Standardized Precipitation Index over Zambia. *Atmosphere* **2020**, *11*, 1268. [[CrossRef](#)]
71. Wang, F.; Yang, H.; Wang, Z.; Zhang, Z.; Li, Z. Drought Evaluation with CMORPH Satellite Precipitation Data in the Yellow River Basin by Using Gridded Standardized Precipitation Evapotranspiration Index. *Remote. Sens.* **2019**, *11*, 485. [[CrossRef](#)]
72. Almazroui, M.; Şen, Z. Trend Analyses Methodologies in Hydro-meteorological Records. *Earth Syst. Environ.* **2020**, *4*, 713–738. [[CrossRef](#)]
73. Ahmed, K.; Shahid, S.; Wang, X.; Nawaz, N.; Khan, N. Spatiotemporal changes in aridity of Pakistan during 1901–2016. *Hydrol. Earth Syst. Sci.* **2019**, *23*, 3081–3096. [[CrossRef](#)]
74. Rahman, G.; Dawood, M. Spatial and temporal variation of rainfall and drought in Khyber Pakhtunkhwa Province of Pakistan during 1971–2015. *Arab. J. Geosci.* **2018**, *11*, 46. [[CrossRef](#)]
75. Bretherton, C.S.; Smith, C.; Wallace, J.M. An Intercomparison of Methods for Finding Coupled Patterns in Climate Data. *J. Clim.* **1992**, 541–560. [[CrossRef](#)]
76. Wallace, J.M.; Smith, C.; Bretherton, C.S. Singular Value Decomposition of Wintertime Sea Surface Temperature and 500-mb Height Anomalies. *J. Clim.* **1992**, 561–576. [[CrossRef](#)]
77. Wu, Z.; Huang, N.E.; Long, S.R.; Peng, C.-K. On the trend, detrending, and variability of nonlinear and nonstationary time series. *Proc. Natl. Acad. Sci. USA* **2007**, *104*, 14889–14894. [[CrossRef](#)] [[PubMed](#)]
78. Wu, Z.; Huang, N.E. Ensemble Empirical Mode Decomposition: A Noise-Assisted Data Analysis Method. *Adv. Adapt. Data Anal.* **2009**, *1*, 1–41. [[CrossRef](#)]
79. Zhu, S.; Remedio, A.R.C.; Sein, D.V.; Sielmann, F.; Ge, F.; Xu, J.; Peng, T.; Jacob, D.; Fraedrich, K.; Zhi, X. Added value of the regionally coupled model ROM in the East Asian summer monsoon modeling. *Theor. Appl. Clim.* **2020**, *140*, 375–387. [[CrossRef](#)]
80. Wu, J.; Zhou, L.; Mo, X.; Zhou, H.; Zhang, J.; Jia, R. Drought monitoring and analysis in China based on the Integrated Surface Drought Index (ISDI). *Int. J. Appl. Earth Obs. Geoinf.* **2015**, *41*, 23–33. [[CrossRef](#)]
81. Roy, S.S.; Roy, N.S. Influence of Pacific decadal oscillation and El Niño Southern oscillation on the summer monsoon precipitation in Myanmar. *Int. J. Clim.* **2010**, *31*, 14–21. [[CrossRef](#)]

82. Kumar, K.K.; Rajagopalan, B.; Hoerling, M.; Bates, G.; Cane, M. Unraveling the Mystery of Indian Monsoon Failure during El Niño. *Science* **2006**, *314*, 115–119. [[CrossRef](#)] [[PubMed](#)]
83. Kreft, S.; Eckstein, D. *Global Climate Risk Index 2014. Who Suffers Most from Extreme Weather Events?* Germanwatch: Bonn, Germany, 2016; ISBN 9783943704143.
84. Delworth, T.L.; Mann, M.E. Observed and simulated multidecadal variability in the Northern Hemisphere. *Clim. Dyn.* **2000**, *16*, 661–676. [[CrossRef](#)]
85. Kerr, R.A. A North Atlantic Climate Pacemaker for the Centuries. *Science* **2000**, *288*, 1984–1985. [[CrossRef](#)] [[PubMed](#)]
86. Bowling, L.C.; Lettermaier, D.P.; Nijssen, B.; Graham, L.P.; Clark, D.B.; El Maayar, M.; Essery, R.; Goers, S.; Gusev, Y.M.; Habets, F.; et al. Simulation of high-latitude hydrological processes in the Torne–Kalix basin: PILPS Phase 2(e). *Glob. Planet. Chang.* **2003**, *38*, 1–30. [[CrossRef](#)]
87. Chang, C.-P.; Zhang, Y.; Li, T. Interannual and Interdecadal Variations of the East Asian Summer Monsoon and Tropical Pacific SSTs. Part I: Roles of the Subtropical Ridge. *J. Clim.* **2000**, *13*, 4310–4325. [[CrossRef](#)]
88. Krishnan, R.; Sugi, M. Pacific decadal oscillation and variability of the Indian summer monsoon rainfall. *Clim. Dyn.* **2003**, *21*, 233–242. [[CrossRef](#)]
89. Zhu, S.; Ge, F.; Sielmann, F.; Pan, M.; Fraedrich, K.; Remedio, A.R.C.; Sein, D.V.; Jacob, D.; Wang, H.; Zhi, X. Seasonal temperature response over the Indochina Peninsula to a worst-case high-emission forcing: A study with the regionally coupled model ROM. *Theor. Appl. Clim.* **2020**, *142*, 613–622. [[CrossRef](#)]
90. Webster, P.J.; Yang, S. Monsoon and ENSO: Selectively Interactive Systems. *Q. J. R. Meteorol. Soc.* **1992**, *118*, 877–926. [[CrossRef](#)]
91. Reckien, D.; Petkova, E.P. Who is responsible for climate change adaptation? *Environ. Res. Lett.* **2018**, *14*, 014010. [[CrossRef](#)]
92. Supari; Tangang, F.; Juneng, L.; Cruz, F.; Chung, J.X.; Ngai, S.T.; Salimun, E.; Mohd, M.S.F.; Santisirisoomboon, J.; Singhruck, P.; et al. Multi-model projections of precipitation extremes in Southeast Asia based on CORDEX–Southeast Asia simulations. *Environ. Res.* **2020**, *184*, 109350. [[CrossRef](#)]